

Obtuse Triangular Billiards II: 100 Degrees Worth of Periodic Trajectories

Richard Evan Schwartz *

August 19, 2008

Abstract

We give a rigorous computer-assisted proof that a triangle has a periodic billiard path provided all its angles are at most 100 degrees.

1 Introduction

1.1 Background

The theory of billiards on rational polygons – i.e. polygons whose angles are all rational multiples of π – is a well-studied subject with deep connections to areas such as Teichmuller theory. See [G], [MT], and [T] for some surveys on billiards, mainly rational. Very little is known about irrational polygonal billiards. Here is a basic conjecture.

Conjecture 1.1 (Triangular Billiards Conjecture) *Every triangle has a periodic billiard path.*

By *triangle* we mean a solid triangular region of the plane. I think it is fair to say that this 200-year-old problem is widely regarded as impenetrable.

In order to survey some results related to the Triangular Billiards Conjecture, we introduce a bit of notation. Let T be a triangle, with the shortest edge labelled 1, the next shortest edge labelled 2, and the longest edge labelled 3. Any periodic billiard path in T gives rise to an infinite repeating

* This research is supported by N.S.F. Grant DMS-0305047 and by a Guggenheim Fellowship

word, which records the succession of sides encountered by the billiard path. This periodic word is called the *combinatorial type* of the path.

- In 1775 Fagnano proved that the combinatorial type 123 (repeating) describes a periodic billiard path on every acute triangle.
- It is an exercise to show that 312321 (repeating) describes a periodic billiard path on all right triangles. See [GSV], [H], and [Tr] for some deeper results on right angled billiards.
- Any given rational polygon has a dense set of periodic billiard paths [BGKT]. See also [M]. See [V], or the surveys above, for the connections to Teichmuller theory.
- The papers [GSV] and [HH] produce some infinite families of combinatorial types which describe periodic billiard paths on some obtuse triangles.
- A periodic billiard path on a triangle is called *stable* if a periodic billiard path of the same combinatorial type exists on all nearby triangles. In §2 we explain that stability is a combinatorial property of the word. In [H] it is shown that no right triangle has a stable periodic billiard path.
- My paper [S] proves that any triangle sufficiently close to the 30-60-90 triangle has a periodic billiard path. At the same time, the following “pessimistic” result is proved: For any $\epsilon > 0$ there is a triangle within ϵ of the 30-60-90 triangle that has no periodic billiard path of combinatorial length less than $1/\epsilon$.
- The paper [HS] shows that any sufficiently small perturbation of an isosceles triangle has a periodic billiard path. This result is deceptively hard: we require several infinite families of combinatorial types.

The purpose of this paper is to prove the following result.

Theorem 1.2 (100 Degree Theorem) *Let T be an obtuse triangle whose big angle is at most 100 degrees. Then T has a stable periodic billiard path.*

I discovered this result operating McBilliards, a graphical user interface that Pat Hooper and I wrote for the purpose of studying the Triangular Billiards Conjecture. (McBilliards also inspired [H], [S] and [HS].)

We will prove the 100 Degree Theorem rigorously, using a combination of traditional mathematics and exact integer computation. We recommend that the reader of this paper operate McBilliards while reading the paper. McBilliards really brings the ideas in the paper to life, and also allows the reader to survey the computer-parts of our proof to a very fine level of detail. In §7 we give the reader instructions for accessing and operating McBilliards. For the reader who doesn't want to learn McBilliards, but who still would like a visual guide to the paper, we have written a simple-to-use and stand-alone Java applet that illustrates our proof. See §7 for details.

For the reader who does not want to use either of our programs, I have tried to make the mathematics stand on its own. Also, I have tried to explain the methods sufficiently well that the interested reader could start from scratch and reproduce the result in its entirety. As I explain in the next section, my method of finding the needed periodic billiard paths is rather simple-minded. Someone reproducing the experiment would probably not find exactly the same list of combinatorial types I use, but I would bet that the hypothetical new list would have a lot of overlap with my list. I think that my list is pretty efficient.

My method of verifying that these combinatorial types do the job is rather complicated and idiosyncratic. Some of the complexity in the verification process is probably necessary, but some of it is a result of my needing to get a feasible computation. (I worked quite hard to develop an efficient method.) On much faster computers, the verification algorithms would be simpler. See §4.2, for instance. Perhaps the main point of my verification process is to convince the reader that the result *can* be proved by a finite computation.

One might wonder whether 100 degrees is a natural cutoff for our result. It is not. We stopped at 100 degrees because it is a nice round number. With a lot more effort, we would perhaps get to 105 or 110 degrees. Below we will explain why 112.5 degrees ($= 5\pi/8$ radians) is a very hard barrier to pass. To use an analogy, our approach to the Triangular Billiards Conjecture is a bit like trying to ride a bicycle to the North Pole. It is pretty clear that the approach will come to grief, but it is hard to say in advance exactly where or how. Results like the “pessimistic result” in [S] mentioned above, and also the deeper complications revealed in [HS], indicate some of the difficulties.

1.2 Discussion of the Experiment and the Proof

Let Δ denote the parameter space of obtuse triangles. The point $(x, y) \in \Delta$ represents a triangle with small angles x and y radians. To each combinatorial type W , we can associate the region $O(W)$ consisting of points $(x, y) \in \Delta$ such that W is the combinatorial type of a periodic billiard path on the triangle corresponding to (x, y) . When $O(W)$ is non-empty, we call $O(W)$ an *orbit tile*, or *tile* for short. The periodic billiard path represented by W is stable iff $O(W)$ is a non-empty open set. When $O(W)$ is not an open set, $O(W)$ is contained in a straight line segment. See §2 for details.

Let $S_{100} \subset \Delta$ denote the region corresponding to triangles whose big angle is at most 100 degrees. For convenience we also assume $x \leq y$. Our general method of proof is to cover S_{100} with orbit tiles. We use stable words because the orbit tiles are much larger. Two problems emerge.

Problem 1: Consider a *boundary point* $(0, y) \in \partial\Delta$, with $y \in (0, \pi/2)$. A triangle very near such a point has no short periodic billiard path. See Lemma 3.1 for a proof. Thus, the covering we seek is necessarily infinite.

Problem 2: Our “pessimistic result” from [S] can be restated like this: No neighborhood of the point $p_6 := (\pi/6, \pi/3)$ has a finite covering by orbit tiles. This point corresponds to the 30-60-90 triangle.

While there is no hope of finding a finite cover of S_{100} , because of these two problems (and *a priori* other problems) we nonetheless used McBilliards to find an infinite cover. McBilliards essentially does two things

1. Given $(x_0, y_0) \in \Delta$, and some N , McBilliards finds all stable combinatorial types W of length at most N such that $(x_0, y_0) \in O(W)$. The program makes a depth-first search through the tree of words, pruning any branch of the tree as soon as it is clear that no completion of the corresponding word prefix can result in a periodic billiard path. Setting $N = 50$ gives a quick answer and setting $N = 1000$ takes all day.
2. Given a stable combinatorial type W , McBilliards computes, to specified precision, the orbit tile $O(W)$. As we will discuss in the paper, $O(W)$ is a “finite sided” region, bounded by analytic arcs. We think that $O(W)$ is always connected and simply connected, but we have no proof.

Our experimental method works like this. We initially set (say) $N = 50$ and sample many points in Δ . We first search for all the stable combinatorial types of length at most N corresponding to some given point. Assuming that we find some words, we then plot the corresponding tiles. Now we repeat. Roughly speaking, at any stage of the process, we choose a point that is right in the center of the largest region we have not covered by orbit tiles. When it seems that our searches for $N = 50$ are no longer meeting with any success, we increase N to 100. And so on. One could perhaps automate this process, but we have not done this.

Sometimes, guided by a hunch, we focus on a small “hole” around a particular point. (Other users are likely to develop similar hunches.) In this case, we steadily increase N while zooming into the region of interest. Sometimes we find a finite cover; sometimes we find the initial portion of an infinite sequence of tiles whose union seems to cover the hole; and sometimes we have to give up without being able to draw any conclusion.

Let

$$p_k = \left(\frac{\pi}{k}, \frac{\pi}{2} - \frac{\pi}{k} \right) \in \partial\Delta. \quad (1)$$

p_k corresponds to a right triangle. Our search reveals 5 features.

1. Solving Problem 1, we found an infinite union of tiles that covers a neighborhood P_3 of the segment $\{0\} \times [5\pi/9, \pi/2]$. Here $5\pi/9$ radians is 100 degrees.
2. The point p_4 presents a minor inconvenience. It seems that no neighborhood of this point in Δ is contained in an orbit tile. However, we cover a neighborhood P_4 of this point by a union of 9 orbit tiles. (For $P_4 \cap S_{100}$ we just need 5 orbit tiles.)
3. The point p_5 presents a similar inconvenience. We cover a neighborhood P_5 of this point by a union of 2 orbit tiles.
4. Solving Problem 2, we found an infinite family of orbit tiles whose union covers a neighborhood P_6 of p_6 . We establish this result in [S].
5. Any point in $S_{100} - (P_3 \cup P_4 \cup P_5 \cup P_6)$ is contained in one of 215 orbit tiles $O(W_7), \dots, O(W_{221})$. The maximum word-length is 184.

Once we have established the listed results, we just have to show that

$$S_{100} \subset \bigcup_{i=3}^{221} P_i. \quad (2)$$

We introduce “dummy” polygons P_1 and P_2 that cover $\Delta - S_{100}$. Thus, Equation 2 is equivalent to

$$\Delta \subset \bigcup_{i=1}^{221} P_i. \quad (3)$$

Establishing this result is a purely combinatorial result. We have a finite number of polygons and we want to see that they form a covering of Δ .

Referring to Item 1 above, P_3 is a certain triangular region in the parameter space. The infinite family of words corresponding to the tiles covering P_3 grows in a very predictable way, and we will use analytic techniques to deal with all the words at once. The method we use here for P_3 is similar to the method we use for P_6 in [S].

The computer-aided portion of our proof deals with Items 2,3 and 5. To explain the general idea, we concentrate on Item 5. For each word W_j we will produce a polygon $P_j \subset O(W_j)$. We choose P_j so that it has dyadic rational vertices. We also choose the polygons P_1, \dots, P_6 to have dyadic rational vertices. Choosing dyadic rational coordinates is useful for technical purposes, as we somewhat explain below.

In §4 we will explain how we check, with a finite amount of computation, that $P_j \subset O(W_j)$. Without giving much of an idea of the actual method, perhaps we can explain why this really is a finite computation. Starting in $O(W_j)$ and moving towards $\partial O(W_j)$, the corresponding billiard path “disappears” in one of finitely many ways. Essentially, some portion of the (geometrically changing) path has to crash into a vertex of the (geometrically changing) triangle. We just have to show that none of these finitely many bad events occurs when we move around the smaller P_j .

For the purposes of giving a proof, it doesn’t matter how we produce our polygons. However, it seems worthwhile to explain the general idea behind our choices. We plot $O(W_j)$ to high precision. We then select a dyadic rational polygon $P_j \subset O(W_j)$ roughly according to 3 criteria.

- P_j must be fairly well contained inside $O(W_j)$, so that a relatively small amount of computation reveals that $P_j \subset O(W_j)$. It is usually quite hard to verify that points very near the boundary of $O(W_j)$ are actually contained in $O(W_j)$.

- P_j should be a sufficiently close approximation to $O(W_j)$ so that (considering pairs of polygons) P_i and P_j have about the same overlap as W_i and W_j . This condition guarantees what we retain the covering property when we replace $O(W_j)$ by P_j .
- The denominators of the vertex-coordinates are not too large. The largest denominator we use is 2^{17} . Having fairly simple coordinates involved turns out to be useful for our rigorous calculations. The technical difficulty is that we want to make exact integer calculations, but we also need to evaluate trig functions on the vertices of our polygons. To solve the problem, we create a look-up table of rational approximations to $\cos(\pi k/2^n)$ for the relevant pairs (k, n) .

It takes some work to satisfy all these requirements. What helps us tremendously is that the orbit tiles, especially the small ones, are extremely close to being convex polygons. Thus, we can get very nice inner approximations. We produced the final polygons “by hand”, using a special feature of McBilliards designed to help us select, manage, and modify such polygons. We got lucky in that the whole business worked out to a feasible computation.

Now we explain why $5\pi/8$ is a hard barrier to pass. Our region P_3 actually covers a neighborhood of the larger segment $\{0\} \times (5\pi/8, \pi/2]$. However, we have no idea how to cover the neighborhood of any point $(0, y)$ with $y \geq 5\pi/8$. Fairly deep searches by McBilliards reveal interesting infinite patterns of orbit tiles that stop well short of covering any such neighborhood.

1.3 Plan of the Paper

This paper is organized as follows.

- In §2 we will present some basic material about triangular billiards. Some of this theory is well known, and some of it is (probably) new.
- In §3 we deal with P_3 , proving that this polygonal region can be covered by infinitely many orbit tiles. This part of the proof is purely traditional, but of course is heavily inspired by computer experimentation.
- In §4 we explain our basic computational algorithm which verifies an equation of the form

$$P \subset O(W), \tag{4}$$

where P is a polygon with dyadic rational vertices and W is a word. Running this algorithm, we verify that $P_j \subset O(W_j)$ for $j = 7, \dots, 221$.

- In §5 we deal with P_4 and P_5 . For the most part, our treatment of P_4 and P_5 uses the algorithm presented in §4, but we need to intervene occasionally and do some hands-on analysis. For the sake of completeness, we briefly review how we covered the region P_6 in [S].
- In §6 we discuss the main computational issues in the paper. In particular, we explain how we verify Equation 3. We also explain how we reduce all our calculations to integer arithmetic.
- In §7 we provide some operating instructions for McBilliards.

The list of all polygons and words we use seems too long to include in this paper. The complete list resides both in McBilliards and in our companion java applet. Also, our website has a written list of all polygons and words.

1.4 Acknowledgements

I did the initial experiments for this project at the Max Planck Institute in Bonn, during July 2004. I would like to thank the M.P.I. for their hospitality and generous support, and also the Guggenheim Foundation. I would like to thank Mike Boyle, Curt McMullen, Dan Rudolph, Martin Schmoll, Serge Troubetzkoy, and Sergei Tabachnikov for their encouragement, and also for helpful conversations related to this work. I would especially like to thank Pat Hooper, who is my collaborator on McBilliards, for an infinite number of helpful conversations about triangular billiards.

2 Unfoldings and Stability

In this chapter we develop some of the basic theory of triangular billiards. Some of this material is well known, and some of it appears in [S] and [HS].

2.1 Unfoldings

We always work with even-length words. Our convention is that a finite word is meant to be a portion of an infinite periodic word. The infinite periodic word is obtained from the given portion just by repeating it endlessly.

Given a word $W = w_1, \dots, w_{2k}$ we define a sequence T_1, \dots, T_{2k} of triangles, by the rule that T_{j-1} and T_j are related by reflection across the w_j th edge of T_j . Here $j = 2, \dots, 2k$. The set $U(W, T) = \{T_j\}_{j=1}^{2k}$ is known as the *unfolding* of the pair (W, T) . This is a well known construction; see [T]. Figure 2.1 shows an example.

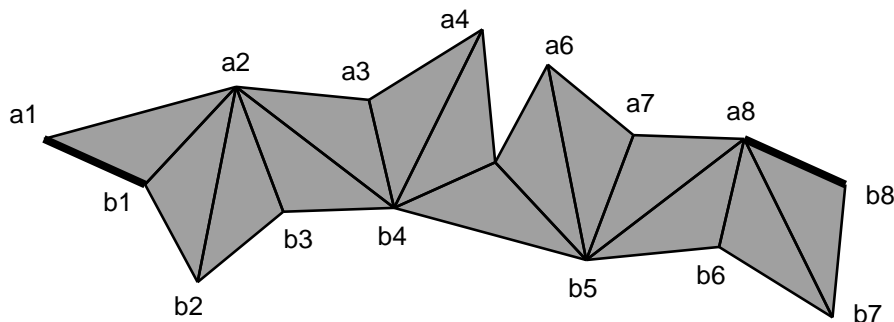


Figure 2.1: The unfolding for $W = (1232313)^2$.

$U(W, T)$ has a *first edge* and a *last edge*. The first edge lies on T_1 and has label w_1 . The last edge lies on T_{2k} and has label w_1 as well. In Figure 2.1, the first edge is the segment joining a_1 to b_1 and the last edge is the segment joining a_8 to b_8 .

W represents a periodic billiard path in T iff the following holds.

1. The first and last edge of $U(W, T)$ are parallel.
2. There is a line segment L joining equivalent interior points on the first and last edges, that remains entirely inside $U(W, T)$. the points.

Here, by *equivalent points* we mean that the translation carrying the one edge to the other identifies the points. When we fold up the line segment, so to speak, it becomes a periodic billiard path on the original triangle. Conversely, a periodic billiard path unfolds into a segment as we have described. The line segment L is never unique. Small parallel translations of L will also satisfy all the hypotheses. We call L a *centerline* for the unfolding. Sometimes we will abuse the terminology and call L *the centerline* even though it is never unique when it exists.

We now describe a labelling convention for the vertices of $U(W, T)$. We can think of $U(W, T)$ as the image in the plane of a polygonal disk $U^*(W, T)$ made by abstractly gluing together triangles as indicated above. The first and last edges of $U^*(W, T)$ make sense as we described them above. Deleting the first and last edges on $U^*(W, T)$, we have two remaining arcs on the boundary $\partial U^*(W, T)$. On one of the arcs we label all the vertices as a_1, a_2, \dots going from the first edge to the last edge. On the other arc we label the vertices as b_1, b_2, \dots going from the first edge to the last edge.

In case the centerline exists, we can rotate so that the centerline is horizontal. In this case our labelling scheme is exactly as in Figure 2.1. All the a vertices lie above the centerline and all the b vertices lie below it. For certain choices of W , called *stable words*, the first and last sides of $U(W, T)$ are always parallel. In this case, we will rotate so that a horizontal translation carries one of these edges to the other. In this case, a centerline exists if and only if all the a vertices lie above all the b vertices.

Remarks:

- (i) Given that our labelling is determined in a combinatorial way, we don't actually need a point in $O(W)$ in order to plot (or estimate) this tile. In practice, we always have such a point, but we don't use it.
- (ii) In the end, we always rotate $U(W, T)$ so that a horizontal translation in the positive horizontal direction carries the first edge to the last. We call this *horizontal position*. However, when we compute certain quantities associated to $U(W, T)$, we initially have $U(W, T)$ in a potentially different position that we call *first position* below.
- (iii) The *unfolding window* on McBilliards shows the unfoldings we have discussed in this section.

2.2 Stability

Recall that a periodic billiard path on a triangle is stable if nearby triangles have a periodic billiard path of the same combinatorial type. As a related notion, we say that a combinatorial type W is *stable* if the first and last sides of $U(W, T)$ are parallel for any triangle T .

Lemma 2.1 *If W is the combinatorial type for a stable billiards path, then W is a stable word. Conversely, if W is a stable word, then any periodic billiard path described by W is stable.*

Proof: Suppose that W describes a stable periodic billiard path on T . Then $U(W, T)$ has a centerline, and the first and last sides are parallel, as discussed above. When we perturb T slightly to a new triangle T' , we still have a periodic billiard path with the same combinatorics. Hence, $U(W, T')$ still has a centerline. In particular, the first and last sides of $U(W, T')$ are still parallel. We have shown that the first and last sides of $U(W, *)$ are parallel for an open set of triangles. But then, by analytic continuation, these sides are always parallel.

Conversely, suppose that W describes a periodic billiard path on T and W is a stable word. When we perturb T slightly, the first and last sides are still parallel, and all the a vertices still lie above all the b vertices. Hence, a centerline still exists. Hence, nearby triangles still have a periodic billiard path described by W . ♠

Remarks:

(i) In our proof, we used analytic continuation as a hammer to smash a pea. Just below, we will see that the parallelism of the first and last sides is a combinatorial condition.

(ii) One can certainly have stable words that describe no periodic billiard paths on any triangle. However, given our method of “search, then plot”, the stable words we find always describe periodic billiard paths on triangles. That is, all the orbit tiles are guaranteed to be nonempty.

The well-known condition that W is a stable word is a combinatorial one. We will describe the stability condition in three equivalent ways. First, we break W into couplets, as we illustrate using the example from the previous section.

$$W = 12 \ 32 \ 31 \ 31 \ 23 \ 23 \ 13.$$

Let N_{ij} denote the number of couplets having type ij . In our example, we have

$$N_{12} = 1; \quad N_{21} = 0; \quad N_{23} = 2; \quad N_{32} = 1; \quad M_{31} = 2; \quad N_{13} = 1.$$

Lemma 2.2 *W is stable if and only if*

$$N_{12} - N_{21} = N_{23} - N_{32} = N_{31} - N_{13}.$$

Proof: Let T_1, \dots, T_{2k} be the triangles in the unfolding $U(W, T)$. We put one more triangle T_0 at the beginning of our unfolding, so that reflection across the first edge maps T_0 to T_1 . The first and last sides (both oriented the same way) are parallel if and only if T_0 and T_{2k} are related by a translation. Let α_j be the angle of our triangle T opposite side j . Looking only at the even triangles of the unfolding, N_{12} counts the number of times a triangle T_j is rotated counterclockwise by $2\alpha_3$ into T_{j+2} . Likewise N_{21} represents the same thing, but in the clockwise direction. The situation is similar for the other quantities. Thus, the angle we rotate T_0 to get to T_{2k} is

$$2(N_{12} - N_{21})\alpha_3 + 2(N_{23} - N_{32})\alpha_2 + 2(N_{31} - N_{13})\alpha_1. \quad (5)$$

The map carrying T_0 to T_{2k} is a translation iff the sum above is an integer multiple of 2π . If our criterion holds, this quantity always equals in integer multiple of 2π . The point here is that $2\alpha_1 + 2\alpha_2 + 2\alpha_3 = 2\pi$. If our criterion fails, then we can produce triangles where the corresponding sum is not an integer multiple of 2π . ♠

Now we will describe stability in a second way. Let \mathcal{H} denote the 1-skeleton of the usual regular hexagonal grid in the plane. \mathcal{H} has 3 parallel families of edges. Given a word, we can draw a path in \mathcal{H} by following the edges as determined by the word: we move along the d th family when we encounter the digit d . We call this path the *hexpath* associated to the word. Figure 2.2 shows the hexpath corresponding the example we have been considering. Note that the hexpath is closed in this case.

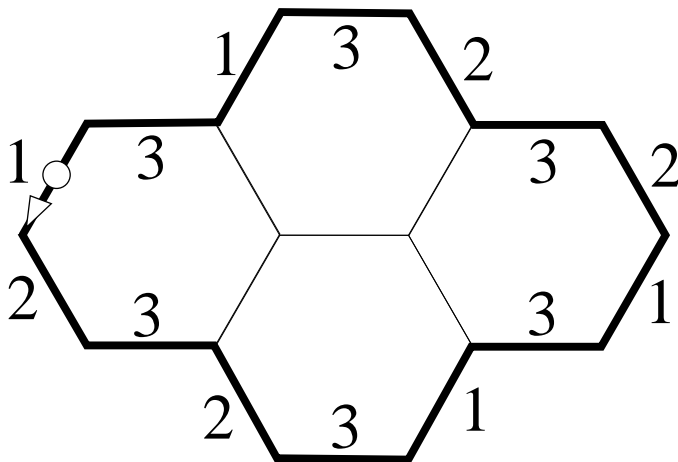


Figure 2.2: The hexpath for $W = (1232313)^2$.

Lemma 2.3 *A word is stable if and only if its hexpath is closed.*

Proof: For this proof, we identify the plane with \mathcal{C} and scale the picture so that opposite sides of each hexagon are 1 unit apart. Considering the hexpath two edges at a time, we see that the location of the final point has the same formula as in Equation 5 except that we replace the angles $\alpha_1, \alpha_2, \alpha_3$ by 3 unit complex numbers, z_1, z_2, z_3 , forming the vertices of an equilateral triangle on the unit circle. An easy exercise shows that the corresponding sum vanishes exactly when our stability condition holds. ♠

Remark: The *word window* in McBilliards draws the hexpaths for the combinatorial types that the search engine finds.

Here we mention one last formulation of the stability condition.

Lemma 2.4 *Let $W = w_1, \dots, w_{2n}$. Let n_{dj} denote the number of solutions to the equation $w_i = d$ with i congruent to $j \pmod 2$. Let $n_d = n_{d0} - n_{d1}$. Then W is stable iff $n_d(W)$ is independent of d .*

Proof: Interpreted in terms of the hexpath, the condition here again says that the hexpath is closed. ♠

2.3 Special Palindromes

We call W a *special palindrome* if W is stable and has the form

$$W = dwd(w^{-1}) \tag{6}$$

Here $d \in \{1, 2, 3\}$ and w is a subword, and w^{-1} is the reverse of w . In this case, $U(W, T)$ has bilateral symmetry, and the translation carrying the first side to the last side of $U(W, T)$ moves perpendicular to these sides.

If $U(W, T)$ has a centerline, then the centerline is necessarily perpendicular to the first and last side. Hence, the corresponding periodic billiard path on T starts and ends perpendicular to one of the sides of T . Conversely, a *stable* periodic billiard path in T with this property has a combinatorial type that is a special palindrome.

Note that there are unstable words that satisfy some but not all of the mentioned properties. For instance 123132 describes an unstable periodic billiard path in any right triangle, and this path starts and ends perpendicular to side 3.

2.4 Turning Angles and Turning Pairs

2.4.1 Definition

Let $U(W, T)$ be the unfolding. Let e_1 be the first edge, oriented so that it points from b_1 to a_1 . We say that $U(W, T)$ is in *first position* if e_1 is parallel to $(0, 1)$. That is, e_1 points in the direction of the positive Y -axis.

Given any oriented edge e of $U(W, T)$, we let $\theta(e)$ denote the angle that one must rotate the positive y -axis counterclockwise so that it coincides with e . Thus, $\theta(e_1) = 0$. In general, $\theta(e)$ is defined mod 2π . The function $\theta(e)$ is really a function of $(x, y) \in \Delta$, and we write this dependence as $\theta(e; x, y)$. It is not hard to see, by induction, that there are integers $M(e)$ and $N(e)$ such that

$$\theta(e; x, y) = M(e)x + N(e)y + \epsilon\pi \quad \text{mod } 2\pi. \tag{7}$$

Here $\epsilon \in \{0, 1\}$. It is sometimes more convenient to consider unoriented edges, in which case we have

$$\theta(e; x, y) = M(e)x + N(e)y \quad \text{mod } \pi. \tag{8}$$

We call $(M(e), N(e))$ the *turning pair* for e . The rest of this section is devoted to explaining how one computes the turning pairs algorithmically.

2.4.2 The Angular Correspondence

First we will give an abstract formulation of how the turning pairs are defined. There is a canonical map from the set of triangles of the unfolding to the set of vertices of the hexpath: We simply map T_i to the i th vertex v_i of the hexpath. The edge of $U(T, *)$ between T_i and T_{i+1} corresponds naturally to the midpoint of the edge joining v_i and v_{i+1} . The other two edges of T_i correspond naturally to the midpoints of the other two edges of \mathcal{H} emanating from v_i . We call this correspondence the *angular correspondence*. For any object of the unfolding X , we let $\Theta(X)$ denote the point in the plane corresponding to X under the angular correspondence. It turns out that there is a real affine transformation R of the plane such that $(M(e), N(e)) = R(\Theta(e))$. This is the abstract formulation.

2.4.3 A Concrete Algorithm

Let d be the first digit of W . For $\epsilon \in \{-1, 0, 1\}$ let $d_\epsilon \in \{1, 2, 3\}$ denote the congruence class of $(d + \epsilon) \bmod 3$. We define

$$\alpha_0(d_\epsilon) = \epsilon; \tag{9}$$

Suppose that we have determined $\alpha_{i-1}(1)$, $\alpha_{i-1}(2)$ and $\alpha_{i-1}(3)$. Let d be the i th digit of W . Define

$$\alpha_i(d_\epsilon) = \alpha_{i-1}(d_\epsilon) + (-1)^i 2\epsilon. \tag{10}$$

In this way we produce a triple of labels for each triangle in the unfolding. If the plane is suitably coordinatized by variables (x, y, z) such that $x + y + z = 0$ then the triple associated to T_i is precisely the coordinates of $\Theta(T_i)$, the i th vertex of the hexpath.

Let e be an edge of $U(W, T)$. Suppose that e is the d th edge of T_i . We define

$$\beta(e, d_\epsilon) = \alpha_i(d_\epsilon) - (-1)^i \epsilon. \tag{11}$$

Note that e could also be an edge of another triangle of $U(W, T)$. This happens when T_{i-1} and T_i are related by a reflection through e . In other words d is the i th digit of W . In this situation Equation 11 gives the same answer whether we use $i-1$ or i in the formula. This can be seen by comparing Equations 10 and 11.

Lemma 2.5 *We have the general formula*

$$\theta(e) = -\frac{\beta(e,1)x + \beta(e,2)y + \beta(e,3)z}{3} \quad (12)$$

Here z is such that $x + y + z = \pi$.

Proof: We first check our formula on the edges of T_1 . If 1 is the first digit of W then the edge labels of e_1 are $(0, 0, 0)$ and hence both sides of Equation 12 are 0. The edge labels of e_2 are $(-1, -1, 2)$. In this case Equation 12 gives $\theta(e_2) - \theta(e_1) = -(-x - y + 2z)/3 = -z$, as it should. The edge labels of e_3 are $(1, -2, 1)$. In this case Equation 12 gives $\theta(e_3) - \theta(e_1) = -(x - 2y + z)/3 = y$, as it should.

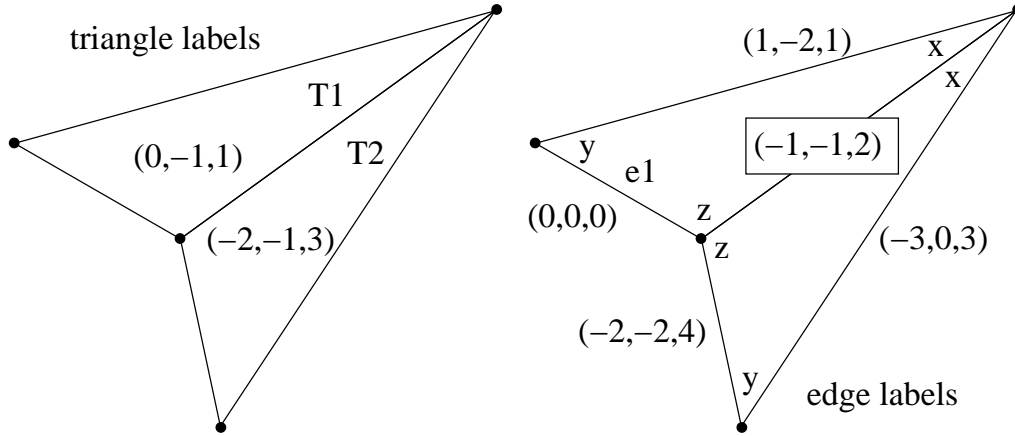


Figure 2.3: Labels for $W = 12\dots$

Given the simple nature of the formulas in Equation 10 and 11 it suffices to check the induction step for $i = 2$. In other words, we just have to see that Equation 12 works for the edges of T_2 . Again, we can suppose that 1 is the first digit of W . Suppose that 2 is the second digit. Figure 2.4 shows a picture of the situation. One easily checks that Equation 12 holds for all these edges. When the second digit of W is a 3 the verification is similar. ♠

It is useful to have a formula that doesn't involve the angle z . We define

$$M(e) = \frac{\beta(e,3) - \beta(e,1)}{3}; \quad N(e) = \frac{\beta(e,3) - \beta(e,2)}{3}. \quad (13)$$

It follows from Lemma 2.5 that $(M(e), N(e))$ is the turning pair for e .

2.5 Defining Functions

Given two points $v, w \in \mathbf{R}^2$ we write

$$v \uparrow w; \quad v \downarrow w; \quad v \downarrow w$$

iff the y coordinate of v respectively is greater than, equal to, or less than the y coordinate of w . In this section we will explain how to define a function f_{uv} such that $f_{uv} > 0$ iff $u \uparrow v$. Here f_{uv} is a function of $(x, y) \in \Delta$. The function f_{uv} has a combinatorial definition, in terms of the positions of u and v on the unfolding. Given these functions, we are left with the following general problem. If $Q \subset \Delta$ is some region and we want to show that $Q \subset O(W)$, we just have to show that $f_{a_i, b_j} > 0$ throughout Q , for all pairs (a_i, b_j) . This explains why the orbit tiles are “finite sided” regions with sides defined by (as we will see) analytic functions.

Let $U(W, T)$ be in first position. Let $\tilde{U}(W, T)$ be the bi-infinite periodic continuation of $U(W, T)$. For any $d \in \{1, 2, 3\}$ there is an infinite, periodic polygonal path made from type- d edges in $\tilde{U}(W, T)$. The image of this path in $U(W, T)$ is what we call the d -spine. Figure 2.4 shows the 3-spine for $U(W, T)$ where T is some triangle of no interest to us. When the first and last sides of $U(W, T)$ are glued together, the d -spine is a closed polygonal loop.

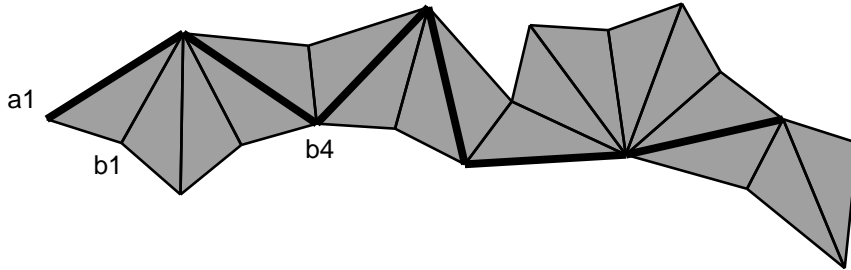


Figure 2.4: The 3-spine for $W = 123231323123232313$.

Let e_1, \dots, e_n be a complete and irredundant list of the edges which appear in the d -spine. We label so that e_1 is the leftmost edge. We introduce the function

$$g_d(x, y) = \sum_{k=1}^n (-1)^{k-1} \exp(i(M(e_k)x + N(e_k)y)). \quad (14)$$

Lemma 2.6 *Suppose that $U(W, T)$ is in first position. The translation direction of $U(W, T)$ is parallel to $\pm ig_d(x, y)$ for any $d \in \{1, 2, 3\}$.*

Proof: Suppose e_1 and e_2 are oriented edges of $U(W, T)$, incident to a common vertex v , and oriented the same way with respect to v . See Figure 2.4. Suppose that e_2 lies to the right of e_1 . Then

$$Mx + Ny \pmod{2\pi}; \quad M = M(e_2) - M(e_1); \quad N = N(e_2) - N(e_1) \quad (15)$$

represents the counterclockwise angle through which e_1 is rotated to produce e_2 .



Figure 2.4: Two edges

We identify the plane with \mathcal{C} . We scale so that the vectors e_1, \dots, e_n of the spine are all unit vectors and the tail vertex of e_1 is 0. We consider two orientations on these edges. Say that the *red* orientation is the one in which the head of each edge hits the tail of the next one. Say that the *blue* orientation is the one where incident edges both point either away or towards the vertex of incidence, as in Figure 2.4.

Let $\rho_k \in \mathcal{C}$ denote the head of e_k minus the tail of e_k , when this edge is oriented according to the red orientation. Likewise define β_k for the blue orientation. The initial point e_1 is 0. The translation we seek carries 0 to the endpoint z of e_n with the red orientation. Thus, our translation carries 0 to

$$\sum_{k=1}^n \rho_k = \sum_{k=1}^n (-1)^{k-1} \beta_k. \quad (16)$$

On the other hand, it follows from induction and Equation 15 that

$$\rho_k = \epsilon \exp(i\tilde{\theta}_k); \quad \tilde{\theta}_k = M(e_k)x + N(e_k)y. \quad (17)$$

Here $\epsilon \in \{-1, 1\}$ is a global sign that does not depend on k . Combining Equations 16 and 17 gives us our result. ♠

Let v and w be two vertices of $U(W, T)$. We say that v and w are d -connected if there is a polygonal path of type- d edges connecting v to w , and d is as large as possible. For instance, if there is a path of type 1 connecting v to w and also a path of type 2 connecting v to w (but no such path of type 3) then we would say that v and w are 2-connected.

Lemma 2.7 *Any pair of vertices are d -connected for a unique $d \in \{1, 2, 3\}$.*

Proof: If d exists, then by definition d is unique. For the existence, let v and w be our vertices. v and w are each incident to two types of vertices. Hence, there is some type, say d , such that v and w are both incident to an edge of type d . We take d as large as possible. Either v lies on the d -spine or else we can connect v to the d -spine with an edge of type d . The same goes for w . Thus, we form our path by connecting v to the d -spine, by travelling along the d -spine, and then by connecting to w . ♠

Let e'_1, \dots, e'_m be the set of type- d edges joining v to w , ordered from left to right. We define

$$h(x, y) = \sum_{k=1}^m (-1)^{k-1} \exp(i(M(e'_k)x + N(e'_k)y)). \quad (18)$$

Lemma 2.8 *Suppose that $U(W, T)$ is in first position. The vector pointing from p to q is parallel to $\pm h(x, y)$.*

Proof: This has almost exactly the same proof as Lemma 2.6. ♠

Letting d be such that v and w are d -connected, we set $g = g_d$.

Lemma 2.9 *Let T be the triangle corresponding to $(x, y) \in \Delta$. Suppose that $U(W, T)$ is in horizontal position. Then the function*

$$f(x, y) = \pm \text{Im}(\overline{g}h) \quad (19)$$

vanishes iff $v \uparrow w$.

Proof: $v \uparrow w$ when $U(W, T)$ is in horizontal position if and only if $g = \overline{g}(x, y)$ and $g = h(x, y)$ are real multiples of each other, which happens iff $\overline{g}h \in \mathbf{R}$, which happens iff $f(x, y) = 0$ ♠

2.6 Getting the Sign Right

Now we discuss the sign in front of Equation 19. We want to use our function to determine when a given vertex lies above another one, and not just when two given vertices are at the same height. That is, we would like to know which sign choice guarantees that $f(x, y) > 0$ iff $v(x, y) \uparrow w(x, y)$. Here we emphasize that the positions of v and w depend on a parameter $(x, y) \in \Delta$.

There are two approaches we might take. One approach is to just make a guess in any given case, and then to use a single auxilliary computation for some point (x_0, y_0) to correct the guess if necessary. By continuity, if the sign is right (or wrong) at one parameter it is right (or wrong) at all parameters. Given that the computer aided portion of our proof only involves a finite number of these functions, we could easily have taken this approach.

The approach we actually take is to establish some general sign conventions and follow them. After an embarrassingly huge amount of trial and error we discovered the general rule that allows us to establish and implement our sign conventions. The proof that the sign formula is correct is a matter of induction. We omit the details.

Recall that v lies to the left of w , and e'_1, e'_2, \dots are the edges of our chosen path connecting v to w . Finally, we note that there is a canonical left-to-right ordering on all the edges of the same type.

The d -spine gives a natural ordering to the edges e_1, \dots, e_n – the red ordering in our proof of Lemma 2.6 – and so it makes sense to speak of the left vertex of e_1 . This is the tail vertex of e_1 relative to the red ordering. The left vertex of e_1 is either a_1 or b_1 .

The Sign Rule: Let s be the number of edges on the list e_1, \dots, e_n which lie to the left of e'_1 .

- Suppose the left vertex of e_1 is a_1 . Then $(-1)^s \text{Im}(\overline{g}h) > 0$ iff $v \uparrow w$.
- Suppose the left vertex of e_1 is b_1 . Then $(-1)^s \text{Im}(\overline{g}h) > 0$ iff $v \downarrow w$.

McBilliards uses the Sign Rule as a basis for establishing the following sign conventions:

1. Suppose $v = a_i$ and $w = b_j$. Then $f > 0$ iff $v \uparrow w$.
2. Suppose $v = a_i$ and $w = b_j$ and $i < j$. Then $f > 0$ iff $w \uparrow v$.
3. Suppose $v = b_i$ and $w = b_j$ and $i < j$. Then $f > 0$ iff $w \uparrow v$.

2.7 Notation

We introduce a shorthand notation for the function f . It suffices to list the turning pairs defining h and then the turning pairs defining g . For instance, in the example above the defining function for the pair (a_1, b_4) is recorded as

$$\begin{array}{cc} 0 & 1 & 0 & 1 & (+) \\ 4 & 1 & 4 & 1 & \\ 4 & -1 & & & \\ 6 & -1 & & & \\ 6 & -3 & & & \\ 0 & -3 & & & \end{array}$$

Here $m = 2$ and $n = 6$. The $(+)$ indicates the sign choice. From the notation we read off that

$$g(x, y) = \exp(i(y)) - \exp(i(4x + y)) + \exp(i(4x - y)) - \dots - \exp(i(-3y)).$$

$$h(x, y) = (+1) \times (\exp(i(y)) - \exp(i(4x + y)));$$

We call this *form 1* for the defining function.

To arrive at a second convenient form for our function we multiply \bar{g} and h together, collect the terms, and use the fact that sine is an odd function. This gives us what we call *Form 2* of the defining function:

$$f(x, y) = \sum_k J_k \sin(A_k x + B_k y); \quad J_k \in \mathbf{N}; \quad A_k, B_k \in \mathbf{Z}. \quad (20)$$

Remark: Using the Unfolding Window on McBilliards, the reader can see computations of the turning pairs and defining functions for any given example.

3 The Infinite Families

3.1 The Region of Interest

The region $P_3 \subset \Delta$ has coordinates

$$\left(0, \frac{\pi}{2}\right); \quad \left(0, \frac{3\pi}{8}\right); \quad \left(\frac{\pi}{8}, \frac{3\pi}{8}\right) \tag{21}$$

The lightly shaded region in Figure 3.1 is Δ . The darkly shaded region is P_3 . The dotted line indicates roughly the boundary of S_{100} .

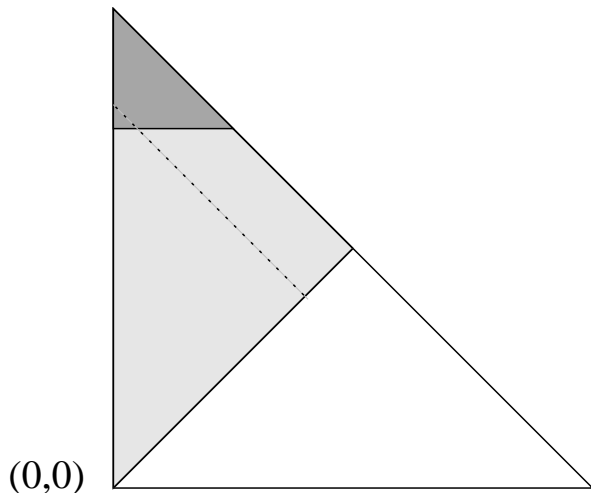


Figure 3.1: The region P_3 .

Lemma 3.1 P_3 has no covering by finitely many orbit tiles.

Proof: Let T be a triangle whose largest angle is $90 + \epsilon$ and whose smallest angle is δ , where $\delta \ll \epsilon$. Any billiard path P in T must eventually hit the short side of T at a point x . But then at least one of the segments S of P , incident to x , will make an angle comparable to ϵ with one of the long sides. Tracing P out from x in the direction of this segment, we see that P has to make about ϵ/δ bounces, moving roughly away from the short side, before its direction can change enough for it to turn around. This shows that T supports no short periodic billiard paths. Hence, we need infinitely many orbit tiles to cover P_3 . ♠

We introduce the words A_n and B_n for $n = 1, 2, 3, \dots$

$$A_n = 3w_n 3w_n^{-1}; \quad B_n = 3w_{n+1} 3w_n^{-1}; \quad w_n = 1(32)^{n+1} 1(23)^n 2 \quad (22)$$

We break P_3 into subregions, each of which is covered by a single tile. Let N_n denote the open triangle bounded by

- The bottom edge of P_3 , namely the line $y = 3\pi/8$;
- The line through $(0, \pi/2)$ having slope $-(n+1)/2$.
- The line through $(0, \pi/2)$ having slope $-(n+2)/2$.

Let N'_n denote the open line segment which is the common boundary of N_n and N_{n+1} . We will prove

$$N_n \subset O(A_n); \quad N'_n \subset O(B_n); \quad n = 1, 2, 3, \dots \quad (23)$$

Figure 3.2 shows the tiles $O(A_1), \dots, O(A_6)$ and the right hand side shows $O(B_1), \dots, O(B_6)$ superimposed over the left hand side. The tiles continue sweeping out to the left, covering P_3 .

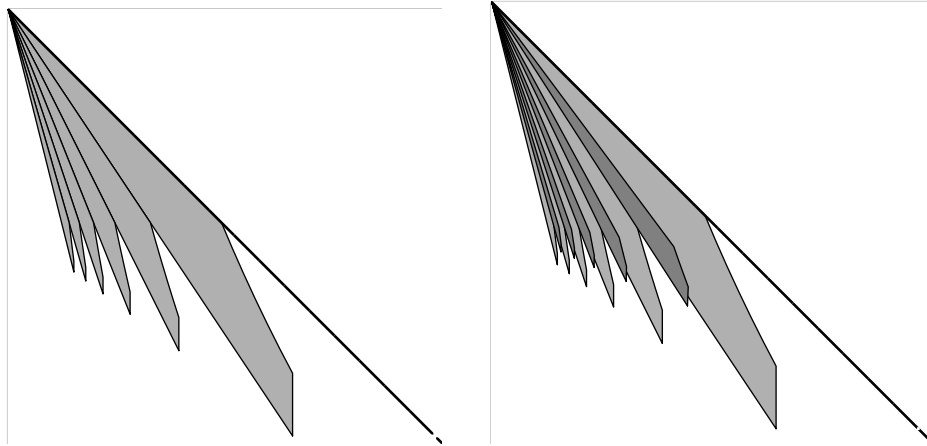


Figure 3.2: Some orbit tiles

We deal with the A tiles first, then the B tiles.

3.2 The A Unfoldings

Figures 3.3-3.5 show unfoldings for A_1 , A_2 , and A_3 respectively, for various choices of triangle. The pattern continues in the obvious way.

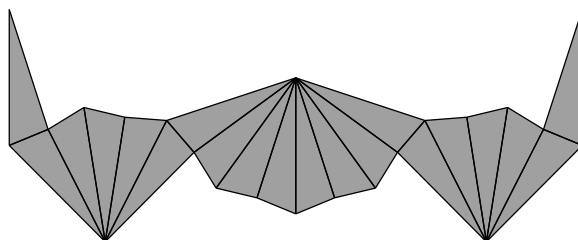


Figure 3.3: Unfolding for A_1 .

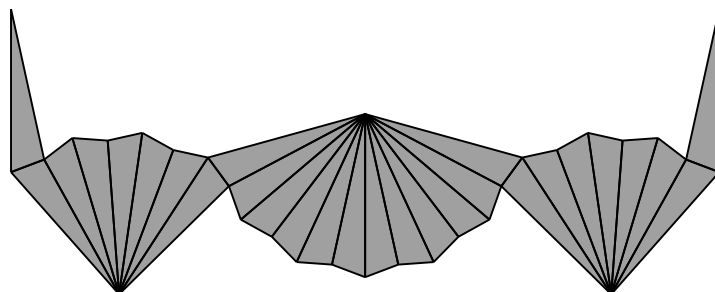


Figure 3.4: Unfolding for A_2 .

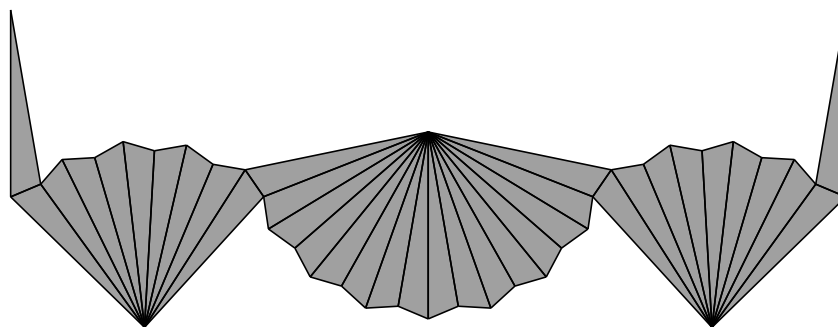


Figure 3.5 Unfolding for A_3 .

3.3 A Special Case

We will concentrate on the case $n = 2$, which is sufficiently complex to contain all the ideas in the proof. At the end we will explain the general case.

Here we analyze the vertices of $U(A_2, T)$, when T corresponds to a point in N_2 . By symmetry it suffices to consider the vertices on the right half of the unfolding. We change our labelling scheme somewhat, and start counting our vertices from the center, as in Figure 3.6. Figure 3.6 shows an enlarged version of Figure 3.4.

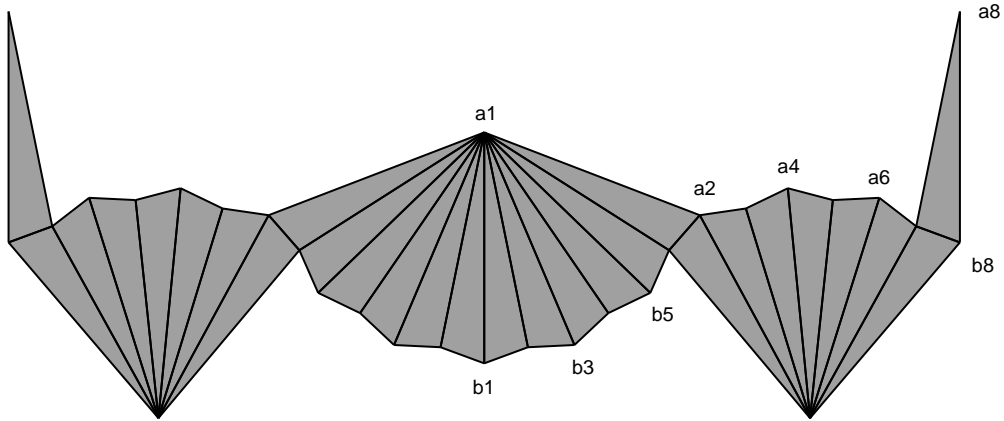


Figure 3.6: Unfolding for A_2 .

Lemma 3.2 *For any $T \in N_2$, and any j , we have $a_j \uparrow a_2$ or $a_j \uparrow a_7$. In other words, the lowest top vertex is either a_2 or a_7 in all cases.*

Proof: Let $\theta(e)$ denote the turning angle of an edge e , as discussed in the previous chapter. We write (for instance) $\theta(a_1b_2) = \theta(\overrightarrow{a_1b_2})$. We let z denote the angle opposite edge 3, so that $x + y + z = \pi$. Here are the angles of importance to us.

$$\theta(a_1a_2) = 6x + \pi; \quad \theta(a_7a_8) = -x; \quad \theta(b_7a_5) = \pi + 3x + 2y \quad (24)$$

We derive the third equation, which is the least obvious. We rotate $\overrightarrow{b_1a_1}$ by $6x$ to get $\overrightarrow{a_2a_1}$. Then we rotate $\overrightarrow{a_2a_1}$ by $2y$ to get to $\overrightarrow{a_2b_7}$. Then we rotate $\overrightarrow{a_2b_7}$ by $-3x$ to get to $\overrightarrow{a_5b_7}$. Then we rotate by π to reverse the direction.

The conditions $(x, y) \in N_2$ give rise to the angle constraints

$$x \in (0, \frac{\pi}{12}); \quad y \in (\frac{3\pi}{8}, \frac{\pi}{2}). \quad (25)$$

See Figure 3.3. From Equation 24 we now get

$$\theta(a_1a_2) \in (\pi, \pi + \pi/2); \quad \theta(a_7a_8) = x \in (-\pi/2, 0) \quad (26)$$

But this means that $a_1 \uparrow a_2$ and $a_8 \uparrow a_7$.

Consider the polygonal “fan” F whose vertices are b_7 and a_3, \dots, a_7 . Note that $\overline{b_7a_5}$ is the line of bilateral symmetry for F . Our constraint $(x, y) \in N_2$ gives

$$\pi - \pi/4 < 2y < \pi - 3x; \quad 3x < \pi/4. \quad (27)$$

Combining these bounds with Equation 24 we get

$$\theta(b_7a_5) \in (\frac{7\pi}{4}, 2\pi) \quad (28)$$

Hence $\overline{b_5a_7}$ has positive slope.

Equation 27 guarantees that F is contained in a halfplane. We can write $F = F_1 \cup F_2$ where F_1 is the convex hull of b_7 and the odd vertices a_3, a_5, a_7 . Then F_2 is a union of 2 small triangles., as shown in Figure 3.7. Given the conditions on F we see that $a_3 \uparrow a_7$ and $a_5 \uparrow a_7$.

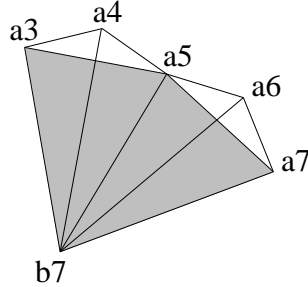


Figure 3.7: The Fan

Since the line of symmetry of F has positive slope and F lies in a half-plane, each even a vertex of the fan lies above one of the adjacent odd a vertices. The point here is that the line segments connecting b_7 to the even vertices are longer than the line segments connecting b_7 to the odd vertices. All in all $a_j \uparrow a_7$ for $j = 3, 4, 5, 6$. ♠

Now we deal with the bottom vertices.

Lemma 3.3 *In all cases, the highest bottom vertex is either b_6 or b_8 .*

Proof: The proof is almost the same as for the top vertices. Let $(x, y) \in N_2$, as above. Since $y < \pi/2$ the line $\overline{b_1b_2}$ has positive slope. Hence $b_2 \uparrow b_1$. To understand the vertices b_2, \dots, b_4 we consider the “fan” whose vertices are $a_1, b_2, b_3, b_4, b_5, b_6$. This polygon is isometric to the one considered in the previous subsection. The line of symmetry of F is $\overline{a_1b_4}$. This line has negative slope because of the fact that $3x < \pi/2$. The same argument as above now shows that $b_6 \uparrow b_j$ for $j = 2, 3, 4, 5$. The angle between $\overrightarrow{b_7b_6}$ and $\overrightarrow{b_7a_5}$ is $4x < \pi/3$. Combining this information with Equation 28 we see that

$$\theta(b_7b_6) \in \left(\frac{7\pi}{4}, \frac{5\pi}{2}\right) \equiv \left(-\frac{\pi}{4}, \frac{\pi}{3}\right). \quad (29)$$

From this we see that $b_6 \uparrow b_7$. ♠

To finish the proof that $N_2 \subset O(A_2)$, we prove the following result.

Lemma 3.4 *When T corresponds to a point in N_2 , we have $a_i \uparrow b_j$ for $i \in \{2, 7\}$ and $j \in \{6, 8\}$.*

Proof: Consider first (a_7, b_8) . We have

$$\theta(b_8a_7) = y \in (0, \pi/2).$$

Hence $a_7 \uparrow b_8$.

Now consider (a_2, b_6) . We have $\theta(a_2b_6) = 4x + y \in (\pi/2, \pi)$. Hence $a_2 \uparrow b_6$.

Now consider (a_2, b_8) . Note that a_2 and b_8 are symmetrically located with respect to our favorite line $\overline{b_7a_5}$. Thus a_2 and b_8 have the same height iff our line is vertical. From Equation 24 and Equation 28 we see that this happens for a point in $\text{closure}(N_2)$ iff $2y + 3x = \pi$. That is, (x, y) has to lie on the right boundary line of N_2 . Equation 28 shows that $a_2 \uparrow b_8$ for $(x, y) \in N_2$.

Now consider (a_7, b_6) . Note that a_7 and b_6 have the same height iff the line $\overline{b_7a_4}$ is vertical. Essentially the same analysis as we have already done shows that our line has negative slope for $(x, y) \in N_2$, and is vertical for $2y + 4x = \pi$. Hence $a_4 \uparrow b_7$. The two points have the same height when (x, y) is in the left boundary of N_2 . ♠

3.4 The General Case

We deal with the top vertices first. The general versions of Equation 24 is

$$\begin{aligned}\theta(a_1a_2) &= (2n+2)x + \pi; & \theta(a_{2n+3}a_{2n+4}) &= -x; \\ \theta(b_{2n+3}a_{n+3}) &= \pi + (n+1)x + 2y\end{aligned}\tag{30}$$

Equation 30 eliminates a_{2n+4} and a_1 from consideration.

The conditions $(x, y) \in N_n$ give rise to the angle constraints

$$x \in (0, \frac{\pi}{4n+8}); \quad y \in (\frac{3\pi}{4}, \frac{\pi}{2}).\tag{31}$$

For $(x, y) \in N_n$ we have

$$\pi - \pi/4 < 2y < \pi - (n+1)x.\tag{32}$$

These equations combine together with Equation 30 to show that the line $\overline{b_{2n+3}a_{n+3}}$ has positive slope. This line is the center of symmetry of the fan with vertices $b_{2n+3}, a_3, \dots, a_{2n+3}$. The same argument as above then shows that a_2, \dots, a_{2n+2} lie above $a_j \uparrow a_{2n+3}$ for $j = 2, \dots, 2n+2$. In this way we eliminate everything but a_2 and a_{2n+3} .

Essentially the same argument eliminates all the b vertices except b_{2n+2} and b_{2n+4} . The key point is that the line $\overline{a_1b_{n+2}}$, which is the line of symmetry for the fan with vertices $a_1; b_2, \dots, b_{2n+2}$, has negative slope. This follows from Equation 31.

The analysis of the edges is the same in the general case. The main points that need to be observed are:

- The points a_2 and b_{2n+4} have the same height iff $\overline{b_{2n+4}a_{n+3}}$ is vertical, and this happens iff $2y + (n+1)x = \pi$.
- a_{2n+3} and b_{2n+2} have the same height iff the line $\overline{b_{2n+3}a_{n+2}}$ is vertical, and this happens iff $2y + (n+2)x = \pi$.

All this information assembles together in the same way as in the case $n = 2$, to show that $N_n \subset O(A_n)$.

3.5 The B Unfoldings

Now we turn to the B tiles. We will draw $U(B_1, T)$ for some triangle T , and then explain the general case.

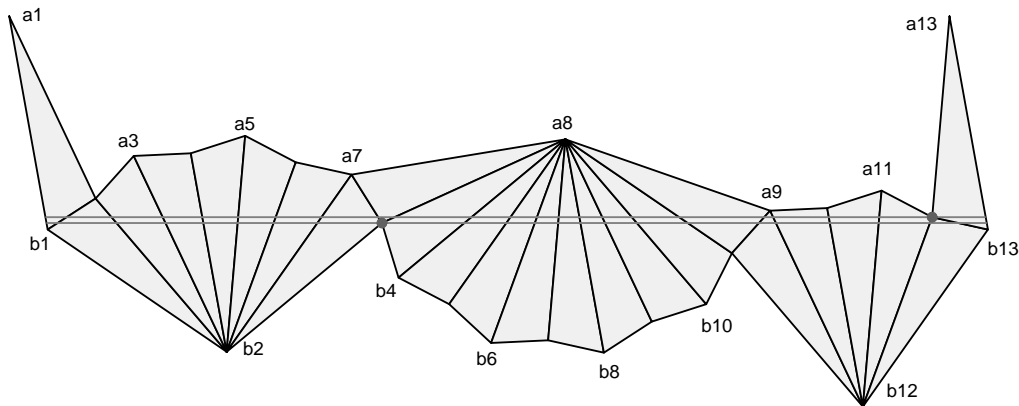


Figure 3.8: Unfolding for B_1 .

Figure 3.8 shows $U(B_1, T)$ for some triangle corresponding to a point $(x, y) \in N'_1$. Such points satisfy the equation

$$3x + 2y = \pi \tag{33}$$

The (near) central edge (a_8, b_8) is parallel to both (a_1, b_1) and (a_{13}, b_{13}) . Indeed the portion of $U(B_1, A)$ to the left of (a_8, b_8) is isometric to the right half of $U(W_2, A)$ and the portion to the right of (a_8, b_8) is isometric to the left half of $U(W_1, A)$. This is fitting, because $O(B_1)$ fits “between” $O(W_1)$ and $O(W_2)$.

In general, $U(B_n)$ is obtained by splicing together the left half of $O(A_n)$ with the right half of $O(A_{n+1})$.

We will take the same approach as for the A tiles. We first consider a special case in detail and then explain the changes needed for the general case. Again, this is entirely for the sake of exposition. We first show that $N'_1 \subset O(B_1)$.

3.6 An Estimate for the Rotation Angle

In the section, we prove

$$\theta(b_{13}a_{13}) \in (0, x); \quad \theta(a_{12}, a_{13}) \in (-x, 0). \quad (34)$$

Lemma 3.5 *There is some $\epsilon > 0$ such that $\theta(a_{12}, a_{13}) \in [0, \epsilon]$ is impossible.*

Proof: The conditions in Equation 33 guarantee that the following lines are parallel

$$\overline{a_{11}b_{12}}; \quad \overline{a_8b_7}; \quad \overline{a_5b_2}; \quad \overline{a_{12}a_{13}}. \quad (35)$$

By symmetry, the points b_{13} and a_3 are related by a reflection in $\overline{a_8b_7}$. The point a_3 and b_1 are related by a reflection in $\overline{a_2b_2}$. If $\overline{a_{12}a_{13}}$ is vertical or has negative slope, then a_3 lies below b_{13} . On the other hand, if $\overline{a_{12}a_{13}}$ is vertical has large negative slope then $\overline{a_2b_2}$ has negative slope. (Here we are using $3x \leq \pi/4$. Compare Equation 27.) But then b_1 lies below a_3 . But then b_1 lies below b_{13} , a contradiction. ♠

Lemma 3.6 *There is some $\epsilon > 0$ such $\theta(b_{13}, a_{13}) \in (-\epsilon, 0]$ is impossible.*

Proof: Condition 33 guarantees that $\overline{a_{10}b_{12}}$, $\overline{a_8b_8}$, $\overline{a_4b_2}$, and $\overline{a_1b_1}$ are all parallel to $\overline{a_{13}b_{13}}$. Let a_0 denote the reflection of a_2 through the line $\overline{a_1b_1}$. Our normalization puts a_0 and a_{12} at the same height. The points a_0 , a_2 , a_6 are successively related to each other by reflections in the lines mentioned above. Likewise, the points a_{12} , b_{11} , b_5 are successively related to each other by reflections in the lines mentioned above. If $\overline{a_{13}b_{13}}$ is either vertical or has sufficiently large negative slope then b_5 lies above a_6 .

The points a_6 and b_3 are related to each other by a reflection through $\overline{b_2a_7}$. The points b_3 and b_5 are related to each other by reflection in the line $\overline{a_8b_4}$. If $\overline{a_{13}b_{13}}$ is either vertical or has sufficiently large negative slope then these two last mentioned lines both have negative slope and hence b_5 lies below a_6 . This is a contradiction. ♠

When x is near 0, the 1-spine of our unfolding converges to a horizontal path. Hence, the two lines $\overline{a_{13}, b_{13}}$ and $\overline{a_{12}, a_{13}}$ converge to vertical lines. By our previous results, these lines have opposite slopes. As we increase x , and remain on N'_1 , this property cannot be lost, by our two results. This establishes our inequalities.

3.7 Most of the Vertices

Lemma 3.7 *For any T corresponding to points in N'_1 , the lowest top vertex is either a_9 or a_{12} . The highest bottom vertex is either b_1, b_3 , or b_{13} .*

Proof: From Equation 34 we get $\theta(a_2a_1) \in (x, 2x)$. Hence $a_1 \uparrow a_2$.

We have $\theta(b_2a_5) = \theta(a_{12}a_{13})$. By Equation 34 we see that $\overline{b_2a_5}$ has positive slope. This line happens to be the line of symmetry for the fan with vertices $b_2; a_3, \dots, a_7$. The same argument as in §3.3 shows that $a_j \uparrow a_7$ for $j = 2, 3, 4, 5, 6$. Similarly, considering the fan with vertices a_8, b_3, \dots, b_{11} , whose line of symmetry $\overline{a_8b_7}$ has positive slope, we see that $b_3 \uparrow b_j$ for $j = 4, \dots, 11$.

Equation 34 gives $\theta(a_7a_8) \in (0, 6x) \in (0, \pi/2)$. Hence $a_8 \uparrow a_7$. Similarly, $b_4 \uparrow b_2$ and $b_{13} \uparrow b_{12}$.

a_7 and a_9 are related by reflection through $\overline{a_8b_7}$, a line with negative slope. Hence $a_7 \uparrow a_9$.

Note that a_{12} and a_{10} are related by a reflection through $\overline{b_{12}a_{10}}$, a line which has negative slope because it is parallel to $\overline{a_{13}b_{13}}$. Hence $a_{10} \uparrow a_{12}$.

a_{12} and a_0 , the point defined in the proof of Lemma 3.6, are at the same height. Moreover, a_0 and a_2 are related by a reflection through the negatively sloped $\overline{a_1b_1}$. Hence $a_2 \uparrow a_{12}$. ♠

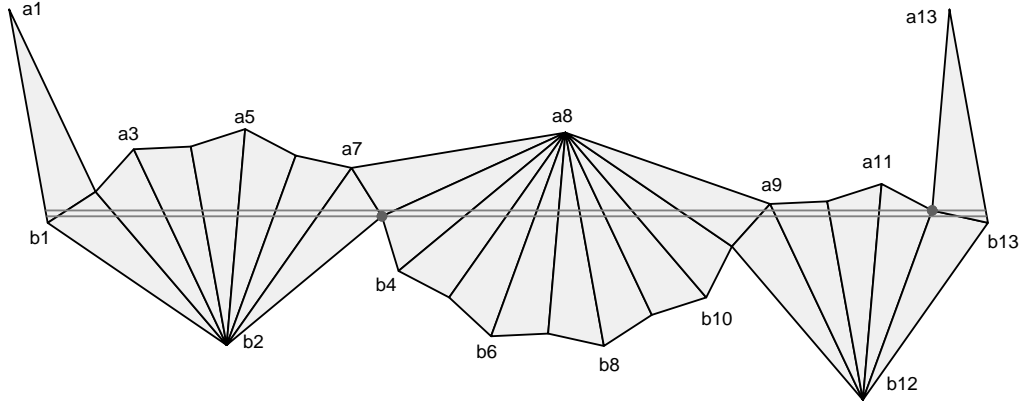


Figure 3.8: Unfolding for B_1 .

3.8 The 6 Pairs

It remains to deal with 6 pairs of vertices. Throughout our argument, we work with triangles corresponding to points in N'_1 .

Lemma 3.8 $a_i \uparrow b_j$ for $i \in \{9, 12\}$ and $j \in \{1, 13\}$.

Proof: Note that b_1 and b_{13} are vertices related by a horizontal translation. Thus, we need not consider b_1 .

We have $\theta(b_{13}, a_{12}) \in (y, x + y)$. We also have $3x + 2y = \pi$. Hence $\theta(b_{13}, a_{12}) \in (0, \pi/2)$. Hence $a_{12} \uparrow b_{13}$.

Consider the pair (a_9, b_{13}) . Since b_{13} and a_9 are related by reflection through $\overline{b_{12}a_{12}}$ and $\theta(b_{12}, a_{12}) = \theta(a_{12}, a_{13}) \in (-x, 0)$ we have $a_9 \uparrow b_{13}$. ♠

It remains to consider the pairs (a_9, b_3) and (a_{12}, b_3) .

Lemma 3.9 a_9 lies above the line $\overline{b_3a_{12}}$. Hence, $a_{12} \uparrow b_3$ implies $a_9 \uparrow a_3$.

Proof: Let θ_1 denote the angle $\angle b_3a_8a_9$. Let θ_2 denote the angle $\angle b_{12}a_9a_{12}$. The point a_9 lies on $\overline{b_3a_{12}}$ iff $(\pi - \theta_2) + \theta_1 = \angle a_8a_9b_{12} = 2y$. Using this fact as a guide, we check signs to determine that a_9 lies above $\overline{b_3a_{12}}$ provided that $\pi - \theta_2 + \theta_1 > 2y$.

Using the law of sines we can normalize so that our triangles all have side lengths $\sin(x), \sin(y), \sin(z)$. Let $\theta_3 = \angle a_9a_{12}b_{12}$. Looking at the triangle with vertices a_3, a_8, b_9 and using the law of sines we get

$$\theta_3 = \frac{\sin(z)}{\sin(y)}\theta_1. \quad (36)$$

Using that the sum of the 3 angles in a triangle is π , together with Equation 33, we get:

$$\theta_1 + \theta_3 = \pi - 9x = \pi - 4 \times 3x + 3x = -3\pi + 8y + 3x = 5y - 3z. \quad (37)$$

The first equation uses Equation 33. Solving for θ_1 we get:

$$\theta_1 = \frac{(5y - 3z) \sin(y)}{\sin(y) + \sin(z)}. \quad (38)$$

Let $\theta_4 = \angle a_9 a_{12} b_{12}$. From the law of sines we have

$$\theta_4 = \frac{\sin(z)}{\sin(y)} \theta_2. \quad (39)$$

We also have

$$\begin{aligned} \theta_2 + \theta_4 &= \pi - 3x = \pi - 2 \times 3x + 3(\pi - y - z) = \\ &= \pi - 2(\pi - 2y) + 3\pi - 3y - 3z = 2\pi + y - 3z \end{aligned} \quad (40)$$

(We have complicated this equation so that it readily generalizes.) Solving for θ_2 we get

$$\theta_2 = \frac{(2\pi + y - 3z) \sin(y)}{\sin(y) + \sin(z)}. \quad (41)$$

Using Equations 38 and 41 we compute

$$(\pi - \theta_2 + \theta_1) - 2b = \frac{(\pi - 2y)(\sin(z) - \sin(y))}{\sin(y) + \sin(z)}. \quad (42)$$

Note that $\sin(z) > \sin(y)$. The expression in Equation 42 is positive as long as $y < \pi/2$, which is certainly our situation. ♠

Lemma 3.10 $a_{12} \uparrow b_3$.

Proof: It is useful to cycle our picture so that b_3 is all the way to the left. See Figure 3.9. Figure 3.9 is cut-and-paste equivalent to Figure 3.8.

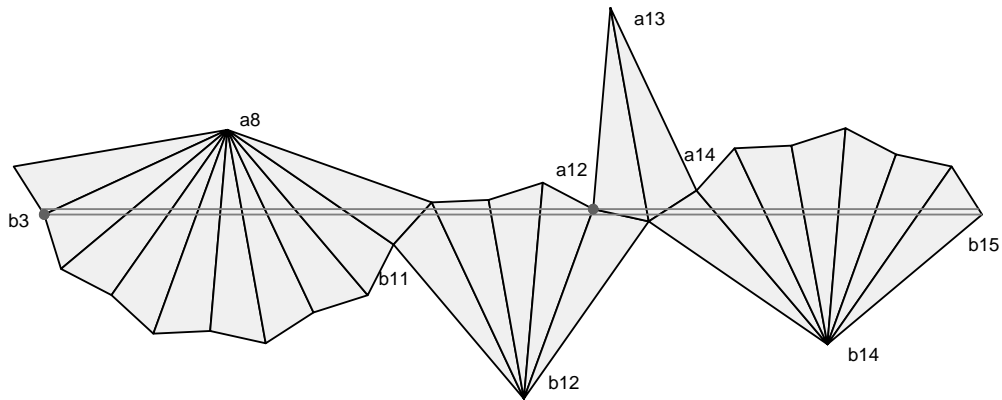


Figure 3.9: Cut and paste

Note that a_{12} lies to the left of both b_{14} and b_{15} . To see this note that a_{14} and b_{15} are related by reflection in the nearly vertical line $\overline{b_{14}a_{17}}$ and a_{14} and a_{12} are related by reflection in the nearly vertical line $\overline{a_{13}b_{13}}$. These lines make an angle of less than x with the vertical, from Equation 34. The same argument shows that b_3 lies to the left of a_{12} .

Let σ_1 and σ_2 respectively denote the slopes of $\overline{b_{15}a_{12}}$ and $\overline{b_3b_{15}}$ when the picture is rotated so that $\overline{b_{15}b_{14}}$ is horizontal. Since a_{12} and b_3 lie to the left of both b_{14} and b_{15} the slopes σ_1 and σ_2 are finite. We will show that $\sigma_1 < \sigma_2$. This, together with the fact that b_3 lies to the left of a_{12} , shows that $a_{12} \uparrow b_3$, as desired.

Consider the path of 8 vectors v_1, \dots, v_8 defined by the vertex sequence

$$(b_{15}, b_{14}, a_{14}, a_{13}, a_{12}, b_{12}, b_{11}, a_8, b_3). \quad (43)$$

In the terminology of §4, this path is part of the 1-spine. The first vector points from b_{15} to b_{14} , and so forth. These vectors all have the same length, which we normalize to be 1.

Let θ_k denote the counterclockwise angle by which v_1 must be rotated to produce v_k . We now calculate these vectors.

Looking at Figure 3.9 have $\theta_1 = 0$ and

- $\theta_2 = 6x + \pi = -4y + \pi$.
- $\theta_3 = 6x - 2z = -4y - 2z$.
- $\theta_4 = 4x - 2z + \pi = -2y + \pi$.
- $\theta_5 = 4x - 4z = -2y - 2z$.
- $\theta_6 = 8x - 4z + \pi = -4y + \pi$.
- $\theta_7 = 8x - 2z = -4y + 2z$.
- $\theta_8 = -2z + \pi$.

In working out some of the equalities we used the relations

$$6x = -4y; \quad 2\alpha_j = -2\alpha_{j-1} - 2\alpha_{j+1}. \quad (44)$$

These relations hold mod 2π , which is all we care about. The first equation comes from Equation 33. To give an example derivation, we will work out the derivations for θ_4 and θ_6 :

$$4x - 2z = 4x + 2x + 2y = 6x + 2y = -4y + 2y = -2y.$$

$$8x - 4z = 12x - 4x - 4z = -8y + (4y + 4z) - 4z = -4y.$$

We want to eliminate x because this is the approach which generalizes to the other words W'_n .

To compute the slope of a point, we divide it's y displacement by it's x -displacement. We set

$$C_k = \sum_{j=1}^k \cos(\theta_j); \quad S_k = \sum_{j=1}^k \sin(\theta_j). \quad (45)$$

Then $\sigma_1 = S_4/C_4$ and $\sigma_2 = S_8/C_8$. Since σ_1 and σ_2 are both finite the terms C_4 and C_8 never vanish. We compute that

$$\sigma_1 - \sigma_2 = \frac{2 \sin(z)}{C_4 C_8} (\cos(z) - \cos(y)). \quad (46)$$

The condition $z \in (\pi/2, \pi)$ makes $\cos(z) < 0$. The condition $y \in (0, \pi/2)$ makes $\cos(y) > 0$. Hence $\sigma_1 - \sigma_2 < 0$. Hence $\sigma_1 < \sigma_2$. ♠

This completes our proof that $N'_1 \subset O(B_1)$. the first tile in the second family.

3.9 The General Case

For N'_n we have the angle condition

$$(n+2)x + 2y = \pi. \quad (47)$$

The proof of Equation 34 works exactly the same way, with the same outcome. Armed with Equation 34 we can use the same arguments as above to eliminate all the pairs of vertices except (b_3, a_{3n+6}) and (b_3, a_{4n+8}) . Figure 3.10 below shows the situation for $n = 2$.

Lemma 3.9 works in general, with the following changes: Equation 37 becomes

$$\theta_1 + \theta_3 = \pi - 4 \times (n+2)x - 3x = 8y - 3x = 5y + 3x. \quad (48)$$

Equation 40 becomes

$$\theta_2 + \theta_4 = 2 \times (n+2)x - 3x = 2(\pi - 2y) - 3(\pi - y - z) = 2\pi + y - 3z. \quad (49)$$

In other words, we get the same equations! The rest of the proof is the same.

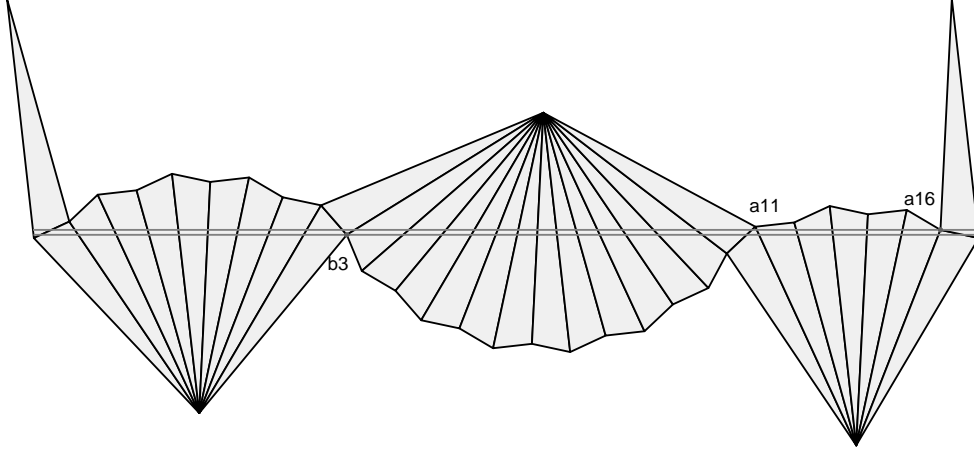


Figure 3.10: Unfolding for B_2 .

The analysis of the pair (b_4, a_{4n+8}) generalizes in the same way. In general, we consider the path of vectors

$$(b_{4n+11}, b_{4n+10}, a_{4n+10}, a_{4n+9}, a_{4n+8}, b_{4n+8}, b_{4n+7}, a_{2n+6}, b_3). \quad (50)$$

The angle sequences we get are

- $\theta_2 = 2(n+2)x + \pi = -4y + \pi.$
- $\theta_3 = 2(n+2)x - 2z = -4y - 2z.$
- $\theta_4 = 2nx - 2z + \pi = -2y + \pi.$
- $\theta_5 = 2nx - 4z = -2y - 2z.$
- $\theta_6 = (4n+4)x - 4z + \pi = -4y + \pi.$
- $\theta_7 = (4n+4)x - 2z = -4y + 2z$
- $\theta_8 = -2z + \pi.$

As above we will show the derivations for θ_4 and θ_6 .

$$2nx - 2z = 2nx + 2x + 2y = (2n+2)x + 2y = -4y + 2y = -2y.$$

$$(4n+4)x - 4z = (4n+8)x - 4x - 4z = -8y + 4y + 4z - 4z = -4.$$

The rest of the proof is the same.

4 The Verification Algorithm

A complete list of the words W_7, \dots, W_{221} and the polygons P_7, \dots, P_{211} resides in 3 places:

- The “100 Degree Result” window in McBilliards. See §7.
- The companion java applet. See §7.
- A written list on my website. My list of publications has a link.

In this chapter we will explain how we verify computationally that

$$P_i \subset O(W_i); \quad i = 7, \dots, 221$$

Here P_i is a given convex dyadic rational polygon and $O(W_i)$ is the orbit tile of a word W_i . The basic algorithm works for indices $i = 30, \dots, 221$. These orbit tiles are contained in the interior of the parameter space Δ . After we describe the basic algorithm, we will explain how it is modified so as to handle the indices $i = 7, \dots, 29$. These indices correspond to orbit tiles that contain a segment on $\partial\Delta$.

Say that a *dyadic rational square* is a square in Δ (the parameter space) whose sides are parallel to the coordinate axes and whose vertices have the form $x(\pi/2)$ where $x \in [0, 1]$ is a dyadic rational.

Our verification algorithm tries to produce a cover of P by dyadic squares $P \subset \bigcup Q_i$, such that $Q_i \subset O(W)$ for all i . To show that $Q \subset O(W)$ we need to show that all the associated defining functions f_{a_i, b_j} are positive on Q . We will sometimes write $f_{ij} = f_{a_i, b_j}$ for ease of notation. In the first section we will explain how we do this. In the sections following the first one, we will explain our main algorithm.

4.1 Certificates of Positivity

Let Q be a dyadic rational square with center q and radius r . Here r denotes half the edge length of Q . Suppose that f is a defining function for a pair of vertices of the unfolding $U(W, T)$. There are two ways we try to certify that $f > 0$ on Q , the *gold* and the *silver*. The gold method is nicer.

4.1.1 The Gold Method

Let $\nabla f = (f_x, f_y)$ be the gradient. From Equation 19 we have

$$f_a = \text{Im}(\bar{g}_a h + \bar{g} h_a); \quad a \in \{x, y\}. \quad (51)$$

We use Equation 20 to get bounds on the second partial derivatives. Using the letters a and b to stand arbitrarily for x and y , we have bounds on the second derivatives:

$$|f_{ab}| \leq F_{ab},$$

where

$$F_{xx} = \sum_k A_k^2 |J_k|; \quad F_{xy} = \sum_k A_k B_k |J_k|; \quad F_{yy} = \sum_k B_k^2 |J_k|. \quad (52)$$

We introduce the quantities

$$a_x = r(F_{xx} + F_{xy}); \quad a_y = r(F_{yx} + F_{yy}). \quad (53)$$

Finally, we define the rectangle

$$G(q, f) = [f_x(q) - a_x, f_x(q) + a_x] \times [f_y(q) - a_y, f_y(q) + a_y]. \quad (54)$$

Here q is the center of Q .

It follows from integration that

$$\nabla f(x, y) \subset G(Q, f); \quad \forall (x, y) \in Q. \quad (55)$$

We say that f is *gold certified* if $G(Q, f)$ is disjoint from the coordinate axes in \mathbf{R}^2 . This is to say that $G(Q, f)$ is contained in one of the standard quadrants in \mathbf{R}^2 .

If f is gold certified, then there is some vertex v of Q such that throughout Q the gradient ∇f is a positive linear combination of the edges of Q which emanate from Q . This means that $f(x, y) > f(v)$ for all $(x, y) \in Q$. Thus, if f is gold certified and $f(v) > 0$ then $f|_Q > 0$. We say that we have shown $f|_Q > 0$ by the *gold method* if this situation obtains. Note that the gold method only requires a finite number of computations. The gold method works poorly if ∇f points nearly horizontally or vertically in Q .

4.1.2 The Silver Method

Let \widehat{Q} denote the square with the following property: Q is midscribed in \widehat{Q} , as shown in Figure 4.1 below. Note that \widehat{Q} is not a dyadic rational because its sides are not parallel to the coordinate axes. However, the vertices and center of \widehat{Q} all have the form πx , where x is a dyadic rational.

We use all the same notation as in the previous section. We not define the rectangle

$$S(q, f) = [f_x(q) - 2a_x, f_x(q) + 2a_x] \times [f_y(q) - 2a_y, f_y(q) + 2a_y]. \quad (56)$$

It follows from integration that

$$\nabla f(x, y) \subset S(Q, f); \quad \forall (x, y) \in \widehat{Q}. \quad (57)$$

We say that f is *silver certified* if $G(Q, f)$ is disjoint from the lines through the origin of slope ± 1 . This is to say that $S(Q, f)$ is contained in one of images obtained by rotating the standard quadrants by 45 degrees.

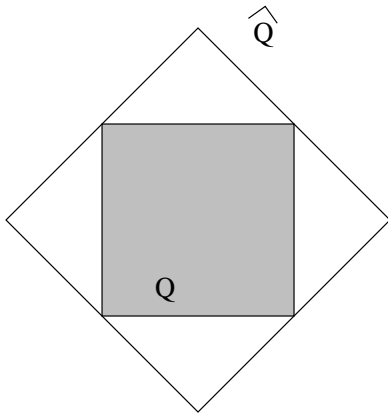


Figure 4.1: Two squares

If f is silver certified, then there is some vertex v of \widehat{Q} such that throughout \widehat{Q} the gradient ∇f is a positive linear combination of the edges of \widehat{Q} which emanate from \widehat{Q} . This means that $f(x, y) > f(v)$ for all $(x, y) \in \widehat{Q}$. In particular, this is true for all $(x, y) \in Q$. Thus, if f is silver certified and $f(v) > 0$ then $f|_Q > 0$. We say that we have shown $f|_Q > 0$ by the *silver method* if this situation obtains. Note that the silver method requires a finite number of computations.

The silver method is not as nice as the gold method for the following reason. If $f|_Q > 0$ but Q is quite close to the level set, then it might happen that $f(v) < 0$ on the relevant vertex of \widehat{Q} . For our purposes, the gold method usually works, and the silver method takes over as

Remark: The constant r in the formulas above has the form $r = \pi x/2$, where x is some dyadic rational number. When it comes time to do our rigorous computation we will replace r by the larger $\tilde{r} = 2x$ because it is a rational quantity. We will then work with the rectangles $\tilde{G}(Q, f)$ and $\tilde{S}(Q, f)$, which are defined as above, but with \tilde{r} in place of r . This replacement makes the functions a bit harder to certify, but helps us reduce the problem to an integer calculation.

4.2 An Inefficient First Try

Here we describe a simple verification algorithm which is too slow to use, but easy to understand. Following this section, we will describe the algorithm we actually do use.

Let Q be a dyadic square and let W be a word. We say that W is *good* on Q if, for every defining function f_{ij} we can prove that $f_{ij}|_Q > 0$ either by the gold method or by the silver method. If W is good on Q then $Q \subset O(W)$.

Let

$$Q_0 = \left[0, \frac{\pi}{2}\right]^2. \quad (58)$$

For our algorithm we start with a list of squares, having the Q_0 as its sole member. At any point of the algorithm we have a list of dyadic rational squares. We let Q be the last square on the list. There are several options.

- If f is good on Q we delete Q from our list and add it to our covering.
- If $Q \cap P = \emptyset$ then we delete Q from our list.
- If neither of the above is true, we replace Q on our list by the 4 squares obtained by subdividing Q in half.

If our list ever becomes empty then we have a covering of P by dyadic squares, each of which is contained in $O(W)$. This does the job. The problem with this algorithm is that it is too slow. We must evaluate all $O(n^2)$ defining functions for each square on the list. Our actual algorithm is similar to the one above, but enhanced so as to be much faster.

4.3 The Tournament

As above, W is a fixed word. Let Q be a dyadic rational square. Say that a *player list* for Q is a pair (A, B) , where both A and B are lists of indices. We think of A as being a list of some distinguished a vertices and B as being a list of some distinguished b vertices. We say that lists $i < j \in A$ are *adjacent* if there is no index $k \in A$ such that $i < j < k$. In this section we will make some definitions for A and at the end make the same definitions for B .

We say that an *A-function* is a defining function associated to (a_i, a_j) , where i and j are adjacent indices in A . We say that a vertex $i \in A$ is an *A-loser* if one of the following two situations (when applicable) obtains:

- Let $j > i$ be the index adjacent to i . Let f be A -function for the pair (a_i, a_j) . Then $-f_Q$ can be certified positive.
- Let $j < i$ be the index adjacent to i . Let f be A -function for the pair (a_i, a_j) . Then f_Q can be certified positive.

One of the situations is not applicable if i is the first or last index in A . If i is the only index in A then neither situation is applicable.

If $i \in A$ is an *A-loser* it means that there is another index $j \in A$ such that $a_i \uparrow a_j$ throughout Q . In this case any result $a_j \uparrow b_k$ in Q automatically implies that $a_i \uparrow b_k$ in Q . If i is not a round loser we call i an *A-survivor*.

We make all the same definitions for the B list, except that we reverse the signs. That is, we say that a vertex $i \in B$ is an *B-loser* if one of the following two situations (when applicable) obtains:

- Let $j > i$ be the index adjacent to i . Let f be B -function for the pair (b_i, b_j) . Then f_Q can be shown to be positive using either the gold or silver method.
- Let $j < i$ be the index adjacent to i . Let f be B -function for the pair (b_i, b_j) . Then $-f_Q$ can be shown to be positive using either the gold or silver method.

We call the following elimination process a *round* (of a tournament): We consider in order all the A -functions f_1, \dots, f_m . We form a new list A' consisting of the A -survivors. We call A *stable* (with respect to Q) if $A' = A$. If A is not stable we form a sequence $A \supset A' \supset A'' \dots$ until the list stabilizes. We call this process the *A-tournament* on Q . We call the indices of the final list the *A-winners*. We carry out the same processes for the B list.

4.4 The Improved Algorithm

We start our algorithm with the list consisting of the triple (Q_0, A_0, B_0) , where $Q_0 = [0, \pi/2]^2$ as above, and $A_0 = B_0 = \{1, 2, 3, \dots, k\}$ are the complete list of indices. Here k is half the length of W . During the algorithm we maintain a list of triples like this. At any stage we consider the last triple (Q, A, B) on the list.

If $Q \cap P = \emptyset$ we discard (Q, A, B) from our list and move on. Otherwise...

- We perform the A -tournament and B -tournament to produce triples (Q, A^*, B^*) , where A^* consists of the A -winners and B^* consists of the B -winners.
- For each index $(i, j) \in A^* \times B^*$ we try to show, using the gold and silver methods, that $f_{ij}|_Q > 0$. If we succeed for every pair then we add Q to our covering of P . Otherwise...
- Delete (Q, A, B) from our list, then replace by the 4 triples (Q_j, A^*, B^*) , where Q_1, Q_2, Q_3, Q_4 are obtained by bisecting Q .

If the list becomes empty then we have produced a covering of P by dyadic squares, each of which is contained in $O(W)$. This is justified by the following result.

Lemma 4.1 *If Q is added to our cover then $Q \subset O(W)$.*

Proof: Let $(i, j) \in A_0 \times B_0$ be arbitrary indices. There is a nested sequence of squares $Q_0 \supset Q_1 \dots \supset Q_n = Q$ together with a sequence of indices $i = i_0, \dots, i_n = i'$ such that $Q \subset Q_k$ and $a_{i_k} \uparrow a_{i_{k+1}}$ for all k . Moreover $i' \in A^*$. The same goes for j in place of i . Therefore, on Q we have $a_i \uparrow a_{i'} \uparrow b_{j'} \uparrow b_j$. ♠

We point out 3 nice features of our algorithm:

- If $P \subset P' \subset O(W)$ and the algorithm works for both P and P' , then the covering produced for P' is obtained from the covering produced for P just by adding some squares.
- The gold and silver certificates are inherited. If a defining function f is gold/silver certified on a square Q it is also gold/silver certified on a subsquare Q' of Q . We don't need to recompute the bounds.

- If Q is one of the squares in our covering, then there is a canonical sequence of squares $Q_0, \dots, Q_n = Q$, where Q_{k+1} is one of the 4 squares in the bisection of Q_k for all k . The presence of Q in our cover can be completely explained by looking at what happens in Q_0, \dots, Q_n . We don't have to look at other "branches" of the algorithm. As we will explain in §7, McBilliards exploits this feature to produce a nice way for the (tireless) reader to inspect the operation of the algorithm piece by piece.

4.5 Exceptional Pairs

Here we explain how to modify our algorithm so that it works in the situation when P_i and $O(W_j)$ both have a segment in common with the right-angled line in $\partial\Delta$

Say that a pair of vertices (a_i, b_j) is *exceptional* if the associated defining function vanishes along the right angle line. We call such a defining function *exceptional* as well. For any word W there is a list A of a vertices of $U(W, *)$ and a list B of b vertices of $U(W, *)$ such that the set of exceptional pairs of vertices is precisely $A \times B$. For the words W_{30}, \dots, P_{229} the lists A and B are typically (though not always) empty. However, the polygons P_{30}, \dots, P_{221} are all (very) disjoint from the right angle line, and so the lists A and B do not concern us. For the words W_7, \dots, W_{29} the lists A and B are always nonempty and, as we mentioned above, the polygons P_7, \dots, P_{29} always have an edge on the right angle line. For this reason, we need to understand what happens with the defining functions associated to vertices in $A \times B$. It is hard to deal computationally with these defining functions, because they take arbitrarily small positive values on points in the polygons.

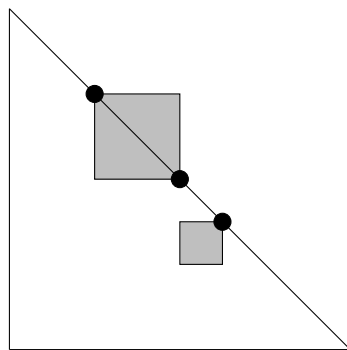


Figure 4.3: Exceptional dyadic squares

Say that a dyadic square is *exceptional* if it has one or two vertices on the right angle line and at least one vertex in the parameter space Δ of obtuse triangles. Figure 4.2 shows a picture of the two kinds of special dyadic squares. Let Q be an exceptional dyadic square and let f be an exceptional defining function. Say that f is *certified* on Q if the gold method shows that ∇f is contained in a quadrant throughout Q we also insist that ∇f points into the obtuse parameter space. In this situation the axis of the quadrant containing ∇f is perpendicular to the right angle line, and $f > 0$ on the portion of Q which lies in Δ .

When we run our algorithm for the indices $i = 7, \dots, 29$ we first isolate the lists A and B . We then run the algorithm as in §5, except that we automatically “pass” any exceptional defining function in the playoffs if the dyadic square in question is exceptional and the defining function is certified on the square. If the algorithm halts, we have a covering of P_i by a union of dyadic squares and dyadic triangles, each of which is contained in $O(W_i)$.

Now we explain how we find special pairs. Each of the exceptional words is a special palindrome. Hence, the first and last edges of $U(W, *)$ are always vertical. This allows us to predict the turning angles of the other edges solely from their turning pairs. Also, we only have to worry about the exceptional pairs involving vertices on the left half of the unfolding.

Figure 4.4 shows the example of W_{11} . In this case, the only exceptional pair of vertices is (a_5, b_1) .

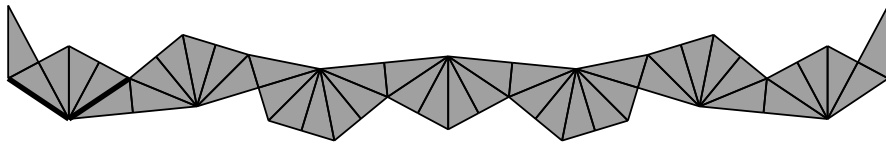


Figure 4.3: Unfolding for W_{11} .

The vertices a_5 and b_1 are joined by 2 edges of type 3. The union of these two edges has a line of bilateral symmetry. Call this line Λ_{51} . The turning pair for Λ_{51} is $(-2, -2)$. Mod π , the angle between the first edge, which is always vertical, and Λ_{51} , is $-2x - 2y$. But $x + y = \pi/2$ on the right angle line. Hence Λ_{51} is vertical for any unfolding with respect to a right triangle. Hence $a_5 \uparrow b_1$ for all points on the right angle line.

Remark: It is not actually necessary for us to show explicitly that we have obtained an exhaustive list of exceptional pairs. We just have to run the modified algorithm and see that it halts, given the exceptional pairs we have singled out. Given that the algorithm is based on finite precision (though exact) arithmetic, another exceptional pair would cause the algorithm to get hung up, producing a list of ever smaller dyadic squares converging to the right-angle line.

4.6 Case by Case Analysis

We recommend that the reader read this part of our analysis while using McBilliards, or the accompanying Java applet. The reader can survey all the unfoldings we discuss and verify that the analysis is correct.

The Easy Cases: With 6 exceptions, the words W_7, \dots, W_{29} have the same analysis as W_{11} . That is, they have a single exceptional pair of vertices (on the left) and the spine connecting these vertices has bilateral symmetry. In all these cases, the same analysis as for W_{11} works here word for word. Here we list these cases, together with the exceptional pairs. Referring to the example in Figure 4.4, the exceptional pair for the word W_{11} is (a_5, b_1) . We denote this by $(11; 5, 1)$. Here are the easy cases:

$$\begin{array}{cccccc}
 (7; 5, 1) & (9; 5, 10) & (10, 5, 1) & (11; 5, 1) & (12; 8, 13) & (13; 1, 11) \\
 (14; 5, 1) & (17; 5, 1) & (19; 19, 3) & (20; 5, 1) & (22; 1, 23) & (24; 27, 5) \\
 (25; 5, 33) & (26; 42, 31) & (27; 38, 7) & (28; 5, 45) & (29; 48, 11) & \\
 \end{array} \tag{59}$$

Notice that the pair (a_5, b_1) occurs quite often. In all cases, the path connecting the vertices in the exceptional pair has the same bilateral symmetry as in Figure 4.5, and the line Λ of bilateral symmetry has turning pair either $(2, 2)$ or $(-2, -2)$ and hence is vertical when the unfolding is done with respect to a right triangle.

The Case of W_8 : Figure 4.5 shows $U(W_8, T)$ for some T . We have highlighted 8 line segments which are all horizontal when x lies on the right angle line. The turning pairs for these segments are all of the form (k, k) for $k \in \{\pm 1, \pm 3, \pm 5\}$. Restricting our attention to the left hand side, we see that the exceptional sets are $A = \{1, 2, 4, 5\}$ and $B = \{8\}$. These are exactly

the ones we single out when we run our algorithm.

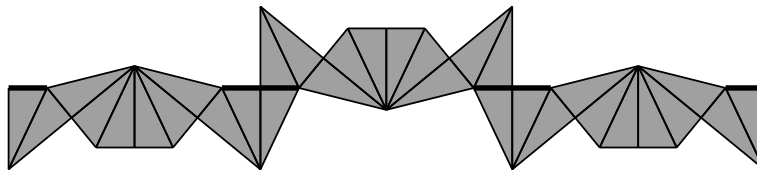


Figure 4.5: Unfolding for W_8 .

The Case of W_{21} : For W_{21} we have $A = \{22, 23\}$ and $B = \{4\}$. In this case, the pair (a_4, b_{22}) has the same kind of bilateral symmetry as for the easy cases. Hence $a_4 \downarrow b_{22}$ for any unfolding with respect to a right triangle. Finally, the turning pair for the edge connecting b_{22} and b_{23} is $(1, 1)$. Hence, this edge is horizontal for any unfolding with respect to a right triangle.

The Cases of W_{16} and W_{23} : For W_{16} we have the lists $A = \{4\}$ and $B = \{7, 8, 14, 15\}$. There is an edge of $U(W_{16}, *)$ connecting a_4 and b_7 , and this edge has turning pair $(1, 1)$. Hence (a_4, b_7) is an exceptional pair. There is an edge connecting b_7 and b_8 and this edge has turning pair $(5, 5)$. Hence $b_7 \downarrow b_8$ on the right angle line. Hence (a_4, b_8) is an exceptional pair. There is a path connecting b_8 to b_{14} which has bilateral symmetry. The line of symmetry contains an edge whose turning pair is $(2, 2)$. Hence $b_8 \downarrow b_{14}$ on the right angle line. Hence (a_4, b_{14}) is an exceptional pair. Finally, there is an edge connecting b_{14} to b_{15} which has turning pair $(-1, -1)$. Hence (a_4, b_{15}) is an exceptional pair.

For W_{23} we have $A = \{12, 13, 29, 30\}$ and $B = \{9\}$. There is an edge connecting b_9 to a_{12} and this edge has turning pair $(-5, -5)$. Hence (a_{12}, b_9) is an exceptional pair. The other 3 pairs are shown to be exceptional as for W_{16} .

The Cases of W_{15} and W_{18} : For W_{15} we have $A = \{1, 2, 4\}$ and $B = \{8, 9, 11, 12, 13\}$. The same arguments as in the previous section show that a_1, a_2, a_4 all lie at the same height when the unfolding is done with respect to a right triangle. The same goes for $b_8, b_9, b_{11}, b_{12}, b_{13}$. Finally, a_4 and b_8 are connected by an edge whose turning angle is $(5, 5)$. Hence (a_5, b_8) is an exceptional pair. Hence all the pairs listed are exceptional.

For W_{18} we have $A = \{1, 2, 4, 5, 6, 8, 9\}$ and $B = \{14, 16, 17, 18\}$. This case is essentially the same as the case of W_{15} .

5 Special Cases

5.1 The Regions of Interest

Figure 5.1 shows a fairly accurate picture of the parameter space Δ of obtuse triangles, as well as the regions P_1, \dots, P_6 discussed in the introduction. The dotted lines indicate that P_1 and P_4 continue “behind” P_2 . It is easier computationally that our union of polygons covers Δ is these two polygons continue as indicated. As we mentioned in the introduction, P_1 and P_2 are just dummy triangles. They don't correspond to periodic billiard paths in triangles. We dealt with P_3 in §3. We dealt with $S' = \Delta_{100} - P_3 - P_4 - P_5 - P_6$ in the §4. Here we deal with P_4, P_5, P_6 . (Actually, we already dealt with P_6 in [S]. Here we just recall what we did.)

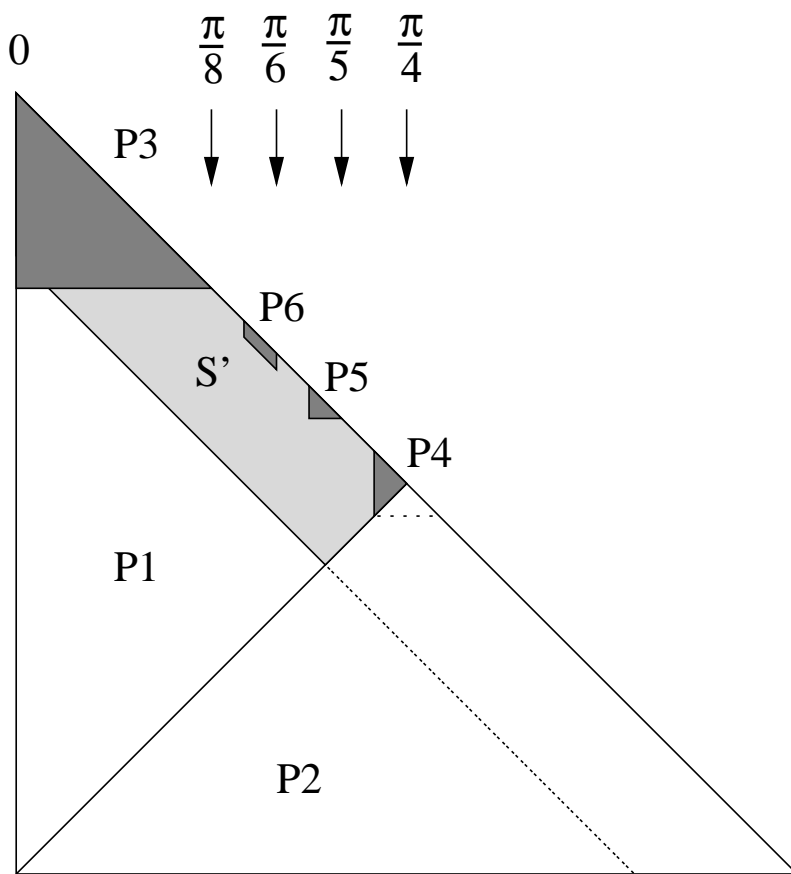


Figure 5.1: Regions in the Parameter Space

We introduce the notation

$$\left| \begin{array}{cc} n_1 & k_1 \\ n_2 & k_2 \end{array} \right| = \frac{\pi}{2} \times \left(\frac{k_1}{2^{n_1}}, \frac{k_2}{2^{n_2}} \right) \quad [\text{example : } \left| \begin{array}{cc} 2 & 1 \\ 2 & 3 \end{array} \right| = \left(\frac{\pi}{8}, \frac{3\pi}{8} \right)] \quad (60)$$

To describe a dyadic polygon, we will list out the vertices. For instance

$$P_4 : \quad \left| \begin{array}{cc} 7 & 63 \\ 7 & 65 \end{array} \right| \left| \begin{array}{cc} 7 & 65 \\ 7 & 63 \end{array} \right| \left| \begin{array}{cc} 7 & 63 \\ 7 & 63 \end{array} \right| \quad (61)$$

$$P_5 : \quad \left| \begin{array}{cc} 12 & 1641 \\ 12 & 2455 \end{array} \right| \left| \begin{array}{cc} 12 & 1637 \\ 12 & 2455 \end{array} \right| \left| \begin{array}{cc} 12 & 1637 \\ 12 & 2459 \end{array} \right| \quad (62)$$

$$P_6 : \quad \left| \begin{array}{cc} 10 & 345 \\ 10 & 679 \end{array} \right| \left| \begin{array}{cc} 12 & 1380 \\ 12 & 2712 \end{array} \right| \left| \begin{array}{cc} 12 & 1352 \\ 12 & 2740 \end{array} \right| \left| \begin{array}{cc} 9 & 169 \\ 9 & 343 \end{array} \right| \quad (63)$$

Here P_k is a tiny region, one of whose boundary components contains the point p_k from Equation 1

5.2 Covering P_6

Let P'_6 denote the region

$$\left\{ (x, y) \in \Delta \mid \left| x - \frac{\pi}{6} \right| < \frac{1}{175}; \quad \left| (x + y) - \frac{\pi}{2} \right| < \frac{1}{400\sqrt{2}} \right\} \quad (64)$$

In [S] we covered P'_6 by a union of two infinite families of orbit tiles. A straightforward computation shows that $P_6 \subset P'_6$.

For the record, we describe the main result here. We used two families of orbit tiles, $\{O(Y_k)\}_{k=8}^\infty$ and $\{O(Z_k)\}_{k=8}^\infty$. The words Y_k are defined for all $k \geq 1$ and the words Z_k are defined for all $k \geq 0$, but we took k fairly large to get better estimates.

We first define the Y family. Let

$$A = 3123; \quad B_1 = 23213; \quad B_2 = 23123; \quad C_1 = 213123; \quad C_2 = 123123. \quad (65)$$

We have $Y_k = 2y_k 2y_k^{-1}$. For odd indices we have

$$y_{2k+1} = AB_1(B_2B_1)^k C_1(B_1B_1)^k; \quad k = 0, 1, 2, \dots \quad (66)$$

For even indices we have

$$y_{2k+2} = AB_1(B_2B_1)^k C_2(B_1B_2)^{k+1}; \quad k = 0, 1, 2, \dots \quad (67)$$

Now we define the Z family. Define

$$A = 123; \quad B = 231; \quad C = 32; \quad D = 213; \quad (68)$$

Next define E_0 to be the empty word and

$$E_1 = DD; \quad E_2 = DAAD; \quad E_3 = DADDAD; \quad E_4 = DADAADAD,$$

and so on. Then $Z_k = 3z_k3z_k^{-1}$, where

$$z_k = ABC3E_kABC \quad (69)$$

(The digit 3 included in the equation is deliberate.)

Figure 5.2 shows the tiles $O(Y_1), \dots, O(Y_4)$. The “tips” of these tiles converge to the point $P(\pi/6)$. The largest tiles $O(Y_1)$ obscures the other tiles. The left vertical grey line indicates the set $y = \pi/6$ and the right grey vertical line indicates the set $y = \pi/5$.

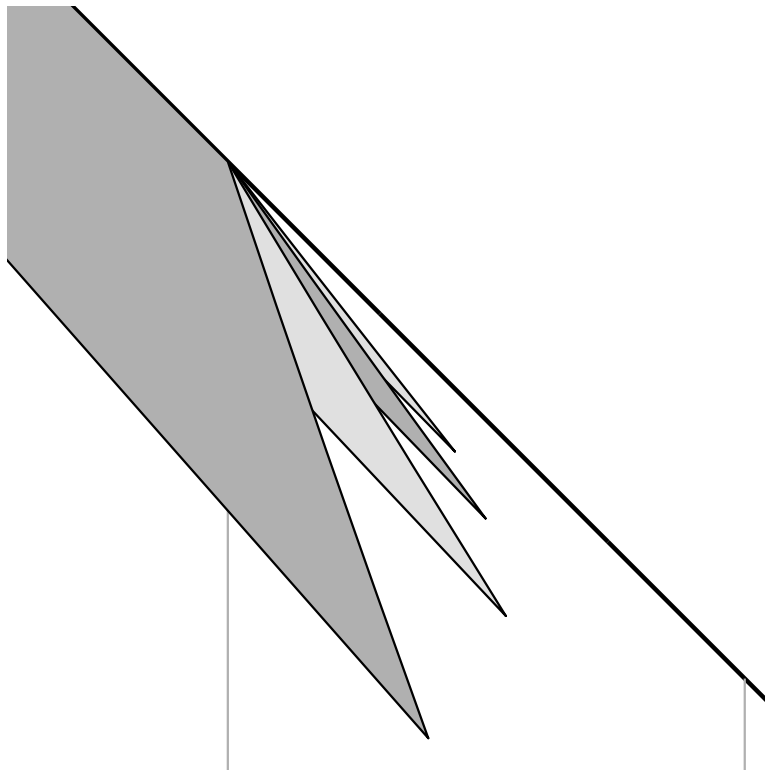


Figure 5.2: The tiles $O(Y_k)$ for $k = 0, 1, 2, 3, 4$.

Figure 5.3 shows how the tiles $O(Y_1), \dots, O(Y_4)$ and $O(Z_0), \dots, O(Z_3)$ interlock and suggests how the neighborhood of $P(\pi/6)$ is filled up.

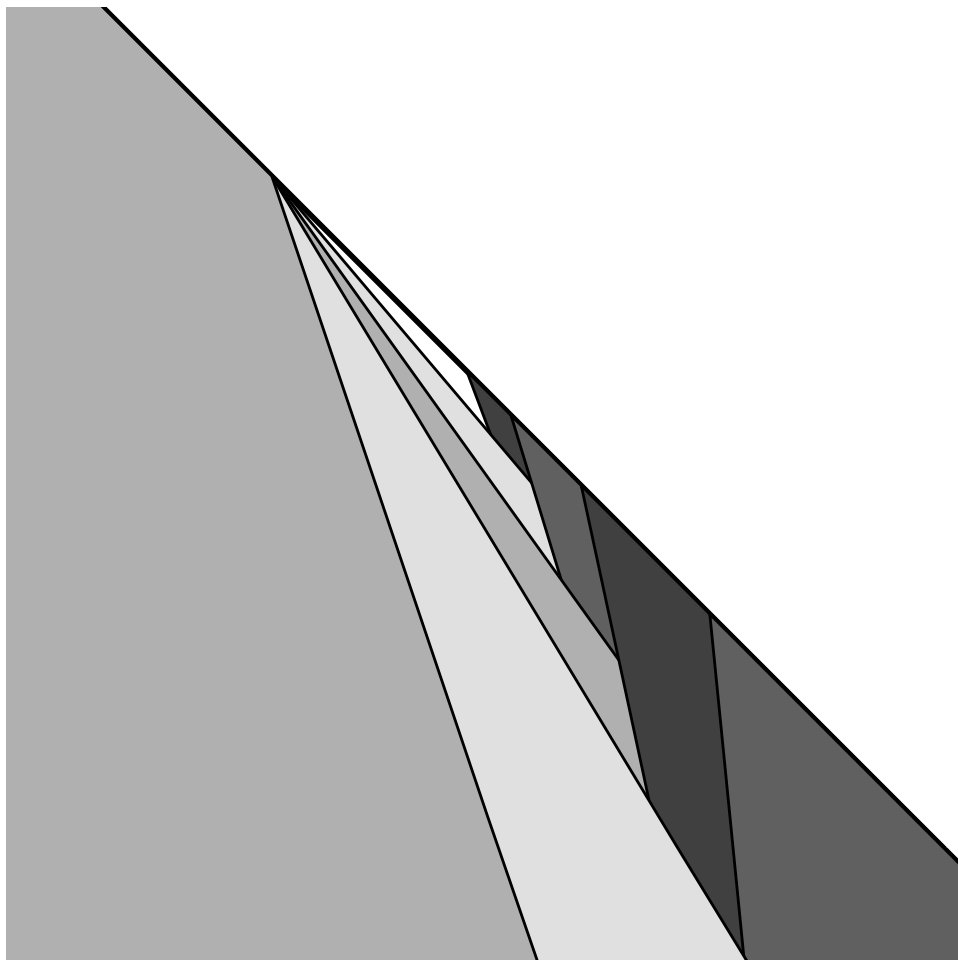


Figure 5.3: Interlocking tiles cover P_6 .

5.3 Covering P_5

Let H_+ denote the half-plane given by $x \geq \pi/5$ and let H_- denote the half-plane given by $x \leq \pi/5$. We consider the words

$$F = 3123231312313232313213132321$$

$$G = 132312323132321321312323132321312312323132321323$$

We will show that

$$P_5 \cap H_+ \subset O(F); \quad P_5 \cap H_- \subset O(G). \quad (70)$$

The basic idea is to check that the verification algorithm described in the previous chapter halts when we ignore certain additional pairs of vertices. Then, at the end, we intervene and analyze the pairs of vertices we ignored.

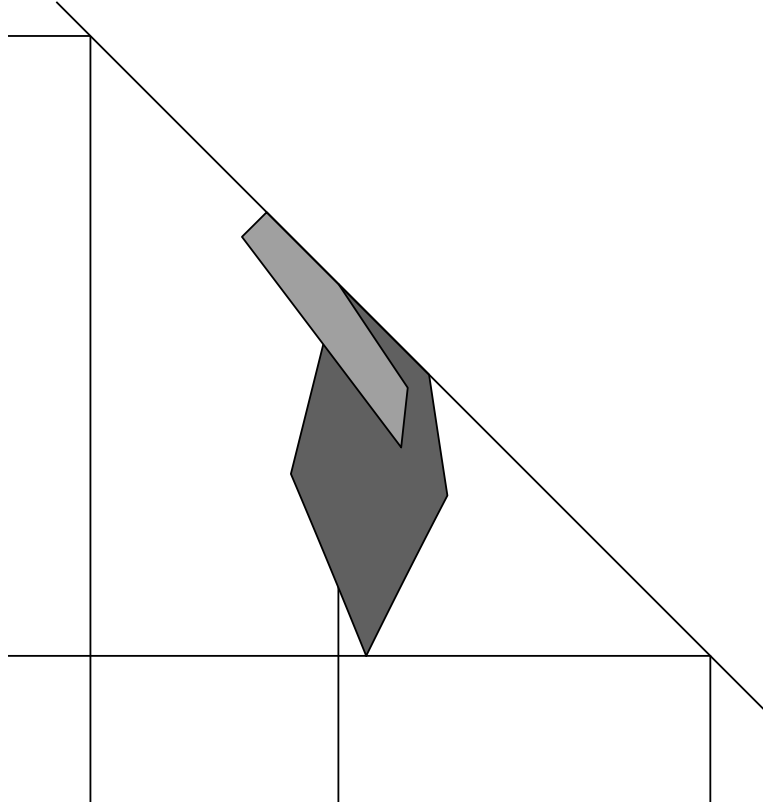


Figure 5.4: Covering P_5 .

5.3.1 Dealing with F

In terms of our listing, we have $F = W_7$, but $P \cap H_+$ is not contained in P_7 . Indeed $P \cap H_+$ shares a vertex with $O(F)$ and we have to work harder. From the list in §4.6, we see that the pair (a_5, b_1) is exceptional. When we also ignore the pairs (a_5, b_5) and (a_5, b_6) we find that our verification algorithm produces a covering of $P_5 \cap H_+$. We already know from our analysis in the previous chapter that $f_{51} > 0$ on P_5 . The point here is that the relevant

line of bilateral symmetry has turning pair $(-2, -2)$ and hence this line has positive slope throughout P_5 . This positive slope forces a_5 to lie above b_1 .

It remains to show that f_{55} and $f_{56} > 0$ on $P_5 \cap H_+$. Figure 5.5 shows a picture of $U(F, T)$ when T is the right triangle corresponding to the point $p_5 \in P_5$.

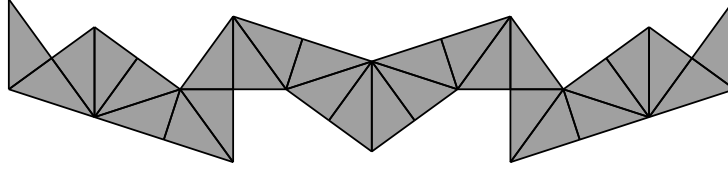


Figure 5.5: The unfolding for F .

The edge connecting a_5 and b_6 has turning pair $(-4, 1)$. Points $(x, y) \in P_5 \cap H_+$ have the form

$$x = \pi/5 + \epsilon; \quad y = 3\pi/10 - \epsilon - \delta.$$

Here ϵ and δ are numbers much smaller than $\pi/10$. The turning angle of the edge connecting a_5 to b_5 is therefore

$$-\pi/2 - 3\epsilon - \delta.$$

This line has negative slope throughout $P_5 \cap H_+$ and hence $a_5 \uparrow b_5$ there.

The vertices a_5 and b_6 are connected by a path of length 2 whose line of bilateral symmetry has turning pair $(-3, 2)$. The corresponding turning angle is

$$-\epsilon - 2\delta.$$

This line has positive slope for $(x, y) \in P_5 \cap H_+$ and hence $a_5 \uparrow b_6$ throughout $P_5 \cap H_+$.

5.3.2 Dealing with G

In terms of our listing, we have $G = W_{13}$. However, $P_5 \cap H_-$ is not a subset of P_{13} so we have to do more work. When we omit the pairs (a_1, b_{11}) and (a_1, b_{12}) and (a_1, b_{13}) our algorithm produces a covering of $P_5 \cap H_-$. It just remains to show that the defining functions associated to these pairs are

positive on $P_5 \cap H_-$. The function $f_{1,11}$ is positive on P_5 for the symmetry reason we discussed in the previous chapter.

Here we explain a proof which works for all 3 defining functions at once. When we run our algorithm, each of these omitted defining functions gets certified on a dyadic square which contains P_5 . We just check that, in all 3 cases, the quadrant which contains the gradients is the $(-, -)$ quadrant. Hence ∇f_{1j} lies in the $(-, -)$. Also, these functions all vanish at p_5 . Every $p \in P \cap H_-$ can be joined to p_5 by a path which points from p_5 into the $(-, -)$ quadrant. Hence $f_{1j} > 0$ on $P \cap H_-$, as desired. Hence $P \cap H_- \subset O(G)$ as desired.

5.4 Covering P_4

Figure 5.6 shows a partition of $P_4 \cap \Delta$ into 5 regions. The regions c, d_1, d_2 are meant to be open. The segments e_1 and e_2 are meant to be open line segments. The 4 solid lines through p_4 have slope $-1, -1/3, 0, \infty$. The dotted line is contained in $\partial\Delta$, and bisects P_4 .

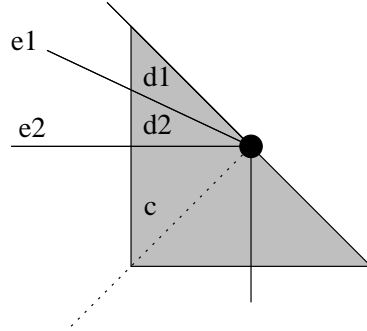


Figure 5.6: Dividing up P_4 .

Since we are taking $x \leq y$ in Δ only the left half of P_4 lies in Δ . We will use the following words.

$$C = (1232313)^2.$$

$$D_1 = 231323123231323123232132313232132313$$

$$D_2 = 2313231323123231323132312323213231323132321323132313$$

$$E_1 = 12323132312323213231323132321323132313231323$$

$$E_2 = 123231323132312323213231323132313232132313231323132313231323$$

The left hand side of Figure 5.7 shows a close-up $O(C)$ and $O(D_1)$ and $O(D_2)$. Note that $O(C)$ slopes over the boundary of $P_4 \cap \Delta$. The boundary here is contained in the line through p_4 of slope 1. (See the dotted line in Figure 7.3.) The large tile $O(C)$ is not completely shown. The union of these three tiles covers all of $P_4 \cap \Delta$ except for two line segments. These two line segments are then covered by $O(E_1)$ and $O(E_2)$, as shown on the right hand side of Figure 5.7.

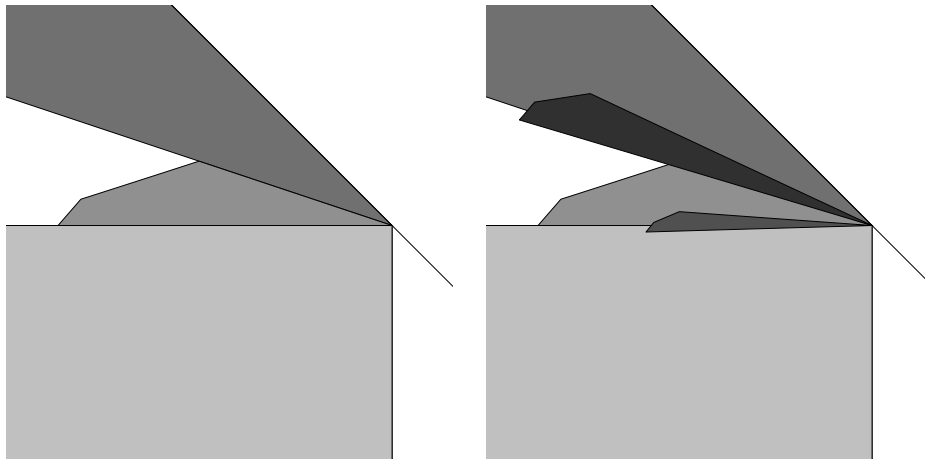


Figure 5.7: Covering P_4

We will prove that $z \subset O(Z)$, for $z \in \{c, d_1, d_2, e_1, e_2\}$.

5.4.1 Dealing with C

In terms of our listing, we have $C = W_{30}$. Let T be the triangle corresponding to the point p_4 , the right isosceles triangle.

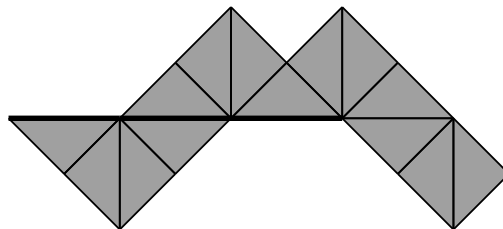


Figure 5.8: $U(C, T)$.

The defining function f_{ij} vanishes at p_4 when $i \in \{1, 2\}$ and $j \in \{4, 5\}$. When we run our algorithm with these vertex pairs excepted, it produces a cover of P by 4 squares. Thus, all the defining functions but the excepted ones are positive on P . The algorithm in this case does not also verify that the gradients of the excepted functions lie in the $(-, -)$ quadrant—this isn't true for f_{14} and f_{25} .

In dealing with the 4 exceptional defining functions, we first compute that

$$|f_{xx}|, |f_{xy}|, |f_{yy}| \leq 2^6.$$

in all cases. We also note that P_4 is contained in a square of radius 2^{-6} . Hence, both $\partial_x f$ and $\partial_y f$ vary by at most 2 units throughout P_4 .

- Here is the formula for f_{15} .

$$\begin{array}{cc|cc} 0 & 1 & 0 & 1 & (-1) \\ 4 & 1 & 4 & 1 & \\ 4 & -3 & 4 & -3 & \\ 0 & -3 & & & \end{array}$$

We compute that $\nabla f_{15}(p_4) = (-8, -8)$. Hence ∇f_{15} lies in the $(-, -)$ quadrant throughout P_4 . Hence $f_{15} > 0$ on the interior of c .

- A similar computation to the one above gives $\nabla f_{24}(p_4) = (-8, -8)$. Hence $f_{24} > 0$ on c .

- Here is the formula for f_{14} :

$$\begin{array}{cc|cc} 0 & 1 & 0 & 1 & (-1) \\ 4 & 1 & 4 & 1 & \\ 4 & -3 & & & \\ 0 & -3 & & & \end{array}$$

We compute that f_{14} vanishes identically along the line $y = \pi/4$. Also, we compute that $\nabla f_{14}(p_4) = (0, -16)$. Hence ∇f_{14} has positive y -coordinate throughout P_4 . Hence $f_{14} > 0$ on c .

- The calculation for f_{25} is just like the one for f_{14} , but with the roles of x and y switched. Hence $f_{25} > 0$ on c .

In summary, all (a, b) defining functions are positive on c . We conclude that $c \subset O(C)$.

5.4.2 Dealing with D_1

In terms of our listing, $D_1 = W_9$. Let T be the right-angled isosceles triangle, as above.

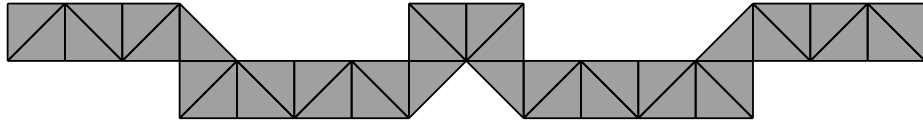


Figure 5.9: $U(D_1, T)$.

Taking i and j on the left half of the unfolding, we see that the defining function f_{ij} vanishes at p_4 iff $i \in \{5, 6, 7, 8\}$ and $j \in \{1, 2, 3, 4, 10\}$. (The center point by convention counts as a vertex on the left half.) When we run the algorithm with these pairs excepted, it produces a covering of P_4 by 3 squares. Once again, the algorithm here does not verify anything about the gradients of the exceptional defining functions.

Reflection in a certain edge e swaps a_6 and a_8 . The turning pair for e is $(2, 2)$. Since the leftmost edge stays vertical for all points in the parameter space, e has negative slope throughout P_4 . Hence $a_6 \uparrow a_8$ throughout P_4 . This eliminates a_6 from consideration.

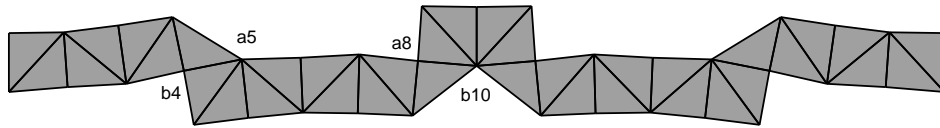


Figure 5.10: $U(D_1, T')$.

Figure 5.10 shows $U(D_1, T')$ where T' is a triangle corresponding to a point of Δ between e_1 and the right angle line. (This point isn't actually in d_1 , because such points give rise to a picture which looks almost identical

to Figure 5.9; we wanted to show the difference dramatically.) Figure 5.10 serves as a reality check to the arguments we give below.

a_6 is connected to a_7 by an edge whose turning pair is $(0, 2)$. As long as $y < \pi/4$ this edge has positive slope and $a_7 \uparrow a_6$. This condition holds in d_1 . This eliminates $i = 7$ from consideration. Similar arguments show that $b_2 \uparrow b_1$ and $b_3 \uparrow b_2$ and $b_3 \uparrow b_4$ throughout d_1 . All in all, we just have to deal with the 4 defining functions f_{ij} where $i \in \{5, 8\}$ and $j \in \{4, 10\}$. Here is the analysis:

- a_8 and b_4 are swapped by reflection in an edge whose turning pair is $(1, 3)$. This edge has positive slope throughout the interior of d_1 , and vanishes on e_1 , the line of slope $-1/3$ through p_4 . Hence $a_8 \uparrow b_4$ throughout d_1 . Hence $f_{84} > 0$.
- a_5 and b_{10} are swapped by reflection in an edge whose turning pair is $(2, 2)$. Hence $f_{5,10} > 0$ on d_1 .
- b_4 and a_5 are connected by an edge whose turning pair is $(-2, 4)$. This edge has positive slope in d_1 . Hence $f_{54} > 0$ in d_1 .
- a_8 and b_{10} are connected by an edge whose turning pair is $(0, 2)$. This line has negative slope in d_1 . Hence $f_{8,10} > 0$ in d_1 .

This takes care of all the cases. Hence $d_1 \subset O(D_1)$.

5.4.3 Dealing with D_2

In terms of our listing, $D_2 = W_{87}$. The analysis of D_2 is almost identical to the analysis of D_1 . We will omit most of the details, but illustrate the main ideas with pictures. Figure 5.11 shows $U(D_2, T)$.

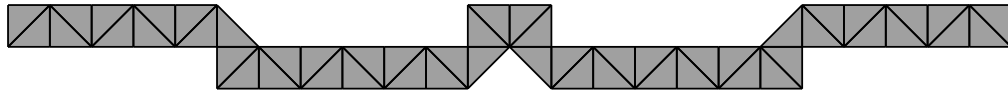


Figure 5.11: $U(D_2, T)$.

Figure 5.12 shows $U(D_3, T')$. Here T' is a triangle corresponding to a point which lies between the lines e_1 and e_2 . (We have gone outside d_2 to get a more dramatic picture.)

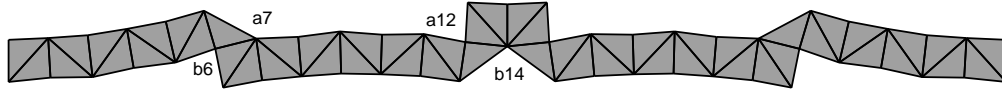


Figure 5.12: $U(D_2, T')$.

When we except all the index pairs entailed by Figure 5.11 our algorithm produces a covering of P_4 by 4 squares. Using the turning pair arguments, as for D_1 , we eliminate all the indices except $i \in \{7, 12\}$ and $j \in \{6, 14\}$. Figure 5.12 is a typical picture of the signs of the slopes of the relevant. These 4 defining functions have the same analysis as for D_1 .

5.4.4 Dealing with E_1

In terms of our listing, $E_1 = W_{107}$. Recall that e_1 is the intersection of the line of slope $-1/3$ through p_4 with P_4 . Figure 5.13 shows a picture of $U(E_1, T)$. When we run our algorithm with all the excepted vertices, it produces a covering of P_4 by 47 squares. We also check, during the algorithm, that ∇f has positive dot product with the vector $(-3, 1)$ throughout P_4 whenever f is an exceptional defining function. This shows that all the exceptional defining functions are negative on e_1 . Hence $e_1 \in O(E_1)$.

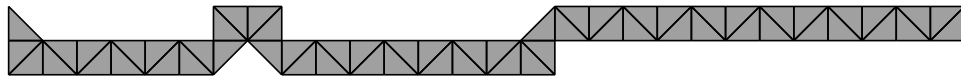


Figure 5.13: $U(E_1, T)$.

Remark: Our gradient check is just a small tweak of the silver method. We compute ∇f , then add all the error bounds coming from the second partials, and check that the entire “error box” makes positive dot product with $(-3, 1)$.

5.4.5 Dealing with E_2

In terms of our listing, $E_2 = W_{85}$.

Recall that e_2 is the intersection of the horizontal line through p_4 with P_4 . Figure 5.14 shows a picture of $U(E_2, T)$.



Figure 5.14: $U(E_2, T)$.

When we run our algorithm with all the excepted vertices, it produces a covering of P_4 by 29 squares. We also check, during the algorithm, that $\partial_x f < 0$ throughout P_4 , whenever f is an exceptional defining function. This shows that all the exceptional defining functions are negative on e_2 . Hence $e_2 \in O(E_2)$.

6 Computational Details

6.1 The Covering Problem

Here we explain how we verify Equation 3. Let P_j be one of the polygons on our list. Let e be an edge of P . We say that e is *good* if

$$e - \partial\Delta \subset \bigcup_{i \neq j} P_i. \quad (71)$$

In case $e \in \partial\Delta$ this condition is vacuous. We say that P_j is *good* if every edge of P_j is good.

Lemma 6.1 $\Delta \subset \bigcup P_j$ provided that every P_j is good.

Proof: If Δ is not covered by our polygons then $\Delta - \bigcup P_j$ contains some open set U and some point of ∂U is contained in some edge e of some P_j . But then e is not good. ♠

To make our problem easier, we scale all our polygons by the constant $2^{27}/\pi$. The result is that all the coordinates of all the polygons are positive integers between 0 and 2^{23} . Also, given the comments at the beginning of §2.7 we know that all the coordinates are divisible by 2^9 . This fact is useful because we sometimes want to subdivide our edges in half a few time, while retaining the property that the break points are integers. We now are left with the problem of showing that a certain convex integer triangle is covered by 221 other convex integer polygons.

The Algorithm: Let S be some segment in the plane, whose endpoints are integers. We call S an *integer segment*. We say that S is *admissible* if the midpoint of S also has integer coordinates. In this case, the two segments S_1 and S_2 formed by bisecting S are also integer segments.

Let e be an edge of P_i . To show that a given edge e is covered by our polygons, we perform the following algorithm. We start with a list of edges whose sole member is e . At any stage of the algorithm we have a finite list of integer segments. We consider the last segment S on the list.

- If we can show that $S \subset P_j$ for some $j \neq i$ then we omit S from our list. Then we continue.

- If S is admissible and we cannot show that $S \subset P_j$ for some $j \neq i$ then we omit S from our list and append S_1 and S_2 to the list. Then we continue.
- If S is not admissible and we cannot show that $S \subset P_j$ for some $j \neq i$ then we fail.
- If the list becomes empty we have succeeded in showing that e is good.

The main step in our algorithm involves showing that an integer segment is contained in an integer convex polygon. This problem in turn boils down to checking that each of the endpoints of the segment is contained in the polygon. Showing that an integer point z is contained in an integer polygon P is an integer calculation. We just check the orientations of all the triangles obtained by coning the edges of P to z and see that they all agree. This calculation is done entirely in \mathbf{Z} and produces integers which have roughly 3 times as many digits as the coordinates of z and P . We implement our algorithm in Java, using the BigInteger class. We discuss this in the next section. The interested reader can see and interact with the cover using McBilliards. In particular, one can re-run our algorithm, either one time at a time or sequentially.

6.2 BigIntegers and BigIntervals

We wrote McBilliards in Java. See www.java.sun.com for information about this language.

The Java programming language has a class called the BigInteger. The BigInteger is an integer, with an “arbitrary” number of base 10 digits. Here “arbitrary” means “subject to the memory limitations of the machine”. Once two BigIntegers are defined, they can be added, subtracted, multiplied, and even exponentiated. If the process of computing the resulting quantity does not exhaust the memory of the machine, then the result is correct. It would probably take integers billions of digits long to exhaust the memory of the machine. In our case we work with integers, all of which have fewer than 200 digits. For this reason, we are convinced that the basic arithmetic operations of the BigInteger class work without fail on the numbers we supply.

Our basic method is to convert all our calculations into integer calculations and then to use BigIntegers to get the calculations exactly right. Our trick is to multiply the naturally computed quantities of interest to us by a

huge integer, namely 2^{106} , and then trap these quantities inside an interval of BigIntegers. We then perform a calculation using BigInteger arithmetic, and in the end produce in interval of BigIntegers which contains 2^{106} times the quantity of interest to us.

The only real-valued functions we compute are the ones in Equation 19 and 20. Once we have these quantities, we do make some further algebraic manipulations, as discussed in connection with the gold and silver methods of §5. However, once we have finished with Equations 19 and 20, we have our intervals of BigIntegers and then we manipulate them as discuss below.

We define a *BigInterval* to be a pair (L, R) of BigIntegers, with $L \leq R$. There are several basic operations which we can perform on these intervals:

- $(L_1, R_1) + (L_2, R_2) = (L_1 + L_2, R_1 + R_2)$.
- $(L_1, R_1) - (L_2, R_2) = (L_1 - R_2, L_2 - R_1)$.
- $(L_1, R_1) \times (L_2, R_2) = (L_3, R_3)$, where $L_3 = \min(L_1L_2, L_1R_2, L_2R_1, L_2R_2)$ and $R_3 = \max(L_1L_2, L_1R_2, L_2R_1, L_2R_2)$.

These operations have the following property: If $x_j \in (L_j, R_j)$ for $j = 1, 2$ then $x_j * y_j \in (L_1, R_1) * (L_2, R_3)$. Here $(*)$ is any of the 3 operations just mentioned. All our calculations boil down to showing that $x > 0$ or $x < 0$ for some real number x . We do our calculations in such a way as to produce a BigInterval (L, R) such that $2^{106}x \in (L, R)$. We would show that $x < 0$ by showing that $R < 0$ and we would show that $x > 0$ by showing that $L > 0$.

6.3 The Interval Cosine Function

Looking at Equations 19 and 51 we see that we need some way to deal with the sine and cosine functions. When we run our subdivision algorithm, we find that it never produces a dyadic square whose side length is less than 2^{18} . For this reason, we are only evaluating the sine and cosine functions on numbers ¹ of the form

$$(\pi/2)\frac{k}{2^{20}}.$$

Using the identities:

$$\sin(x) = \cos(\pi/2 - x); \quad \cos(x + n\pi) = (-1)^n \cos(x)$$

¹Actually we just need 2^{18} rather than 2^{20} but we want to give ourselves a little cushion here.

we see that it suffices to consider the 2^{21} values

$$c_k := 2^{53} \cos(\pi/2 \times \frac{k}{2^{20}}); \quad k = 0, \dots, 2^{21} - 1.$$

(There is nothing special about 2^{53} . We like it because it affords about the same precision as a double in C.)

We now explain how we produce a `BigInterval` I_k such that $c_k \in I_k$. Once we have I_k , we evaluate Equations 19 and 51 using the operations discussed above. Producing I_k is quite easy. The tricky part is proving rigorously that our method really works. We know that there exist packages in Java which perform this task for the elementary functions, but we prefer to work from scratch. We want to stress that it doesn't really matter how we produce our `BigInterval` I_k . The important point is the proof that $c_k \in I_k$. However, it seems worth explaining our simple method.

6.3.1 Producing the Interval

We introduce the routine `cosBestApprox`. When we evaluate this routine on the pair $(k, 20)$ it produces a `BigInteger` C_k . We then take

$$I_k = (C_k - 4, C_k + 4).$$

The routine `cosBestApprox` essentially computes “the usual” cosine on the relevant point—here $n = 20$ and k is as above— and then rounds to the nearest `BigInteger`. Our method uses the `BigDecimal` class, which is just a `BigInteger`, together with a separate integer which tells where to put the decimal point. Here is our code, all of which can be found online in the file `Deg100Trig.java`.

```
public static BigInteger cosBestApprox(int k,int n) {
double d=Math.PI/2.0;
d=d*k/Math.pow(2.0,n);
d=Math.cos(d);
BigDecimal Y1=new BigDecimal(d);
BigInteger BIG=getBIG();
BigDecimal Y2=new BigDecimal(BIG);
Y1=Y1.multiply(Y2);
BigInteger X=Y1.toBigInteger();
return(X);
```

}

The BigInteger BIG is 2^{53} . Here is the routine which gets it:

```
public static BigInteger getBIG() {  
    BigInteger BIG=new BigInteger("9007199254740992");  
    return(BIG); }
```

6.3.2 Checking that the Method Works

What we actually show is that

$$2^{357}20!c_k \in 2^{357}20!I_k.$$

A huge number like this appears fairly naturally because we want to clear denominators in some Taylor series approximations for cosine.

For $j = 0, 1, \dots, 10$ let L_j be the greatest integer less than

$$\frac{2^{400}20!}{2^{40j}(2j)!} \times (\pi/2)^{2j}. \quad (72)$$

Let $R_j = L_j + 1$. We compute these 20 integers using Mathematica, which has a reliable arbitrary precision evaluation of the trig functions. The reader can see our values in the file Deg100Trig.java. Consider the sums

$$A_k = L_0 - R_1k^2 + L_2k^4 - R_3k^6 + \dots - R_{10}k^{20} \quad (73)$$

$$B_k = R_0 - L_1k^2 + R_2k^4 - L_3k^6 + \dots + R_9k^{18} \quad (74)$$

Considering the Taylor series for cosine, we easily get that

$$2^{357}20!c_k \in [A_k, B_k]. \quad (75)$$

To verify that $c_k \in I_k$ it suffices to check that

$$2^{257}20!(C_k - 4) < A_k; \quad B_k < 2^{357}20!(C_k + 4).$$

This is purely a calculation involving BigIntegers. We perform the verification and it works. As a control, we performed the verification using “2” in place of “4” and it failed at some point. The program is contained in the

same file as already mentioned. The reader can launch the program right from the 100 Degree window in McBilliards.

Remark: We found that $2^{357}20!$ worked well for us. This choice yields the following values

- $A_8 = 193117979382323170336391434868704$;
- $A_9 = 1416254196461936667$;
- $A_{10} = 8363$.
- $A_{11} = 0$.

This, the choice $2^{357}20!$ is well adapted to an approximation based on about 10 terms of the Taylor series.

6.4 BigInterval Structures

As one last bit of structure, we define a *BigComplexInterval* to be a structure of the form $X + iY$ where X and Y are BigIntervals. The arithmetic on these objects is just the same as the arithmetic on ordinary complex numbers, except that we substitute the BigInterval operations for the ordinary arithmetic operations on reals. (We never have occasion to do any division, so we are just talking about addition, subtraction, and multiplication.)

Once we have our BigInterval version of sine and cosine, and the BigComplexInterval class, we plug these objects into Equations 19 and 51, wrapping every integer in sight inside a BigInterval. We then perform all the operations described in §5. Our algorithm halts for all 221 polygons and this constitutes our proof of the 100 Degree Theorem.

The reader can run our algorithm and survey its output using McBilliards, as discussed in the paper. In particular, the reader can run the algorithm with or without the BigInterval arithmetic, and see that the output is about the same in both cases. (The output is not exactly the same because we make some convenient but arbitrary cutoffs in the numerical version.)

6.5 Sanity Checks

In order to help insure that we have programmed the computer correctly, we have made 3 additional sanity checks in our calculations.

1. We make sure that our combinatorial method of computing the defining functions, namely Equation 19, is correct. We introduce a straightforward geometric method of computing the defining functions geometrically: We just take the unfolding for the word and the given triangle, rotate it so that it is horizontal, and then measure the difference in heights of the relevant vertices. For each word W_i we evaluate each defining function on the first vertex of the polygon P_i , using both methods. As long as the geometric method yields a number which is at least .001 we check, up to a tolerance of .000001, that there is a single ratio ρ such that the ratio of the combinatorial answer to the geometric answer is always ρ . (This ratio depends on the point of evaluation.) In other words, up to a initial rescaling, the two methods agree. We consider this to be extremely strong evidence that we have got Equation 19 correct, and also programmed it correctly into the computer. We do not consider the very small percentage of defining functions which evaluate to a very small number, because the roundoff error interferes with the computation of the ratio.

2. We make sure that our BigInterval versions of our functions yield essentially the same answers as our numerical versions. We make the same evaluations as for the first sanity check, except now we compare the numerical and BigInterval implementations of the combinatorial method. We check that the first 7 digits of the left endpoint of the BigInterval version agree with the first 7 digits of 2^{106} times the numerical version. In the interest of having the check move along at a steady clip when run from the interface, we only check about 4 percent of the defining functions. This still comes out to a huge number of checks. Unlike the first check, where the point is to verify that all cases of a complicated combinatorial procedure work, here we are just checking a fairly straightforward conversion from ordinary arithmetic operations to BigInterval operations.

3. We make sure that our formula for Equation 51 is correctly implemented. For this purpose we compare the partial derivatives of the defining functions with a crude version of the partial derivatives obtained by taking a difference quotient. Our value of Δx and Δy in this computation is 2^{-30} . We check that the two computations of the partial derivatives agree up to a fractional error of .001. By this we mean that

$|X_1 - X_2|/|X_1| < .001$. Here X_1 and X_2 are the two computed versions of the same quantity. We also require X_1 , which is the difference quotient, to be at least .000001. We test about 1 percent of the defining functions. Given the simple nature of the passage from Equation 19 to Equation 51, this is overwhelming evidence that we have programmed Equation 51 correctly into the computer.

The reader can run our sanity checks, either for individual words or else for all words in sequence, from the 100 Degree window in McBilliards. The code for our sanity checks is contained in the file Deg100SanityCheck.java. Indeed, all our computer code pertaining to the 100 Degree Theorem can be launched from this window.

We also mention another sanity check. Originally we had programmed McBilliards in C and Tcl. We originally did all the computations for this paper in the C version. (We switched to Java so that the whole proof could be easily accessible right on the web, to someone without specialized computer knowledge; and also because we wanted to make a new and improved McBilliards.)

Perhaps the best sanity check of all is that McBilliards *works*. This program has many interlocking features, and the interested reader can see that they all fit together in a way which would be extremely unlikely given serious bugs in the program.

7 Using McBilliards

7.1 The Applet

For the reader mainly interested in seeing the results in this paper illustrated, we recommend the java applet we wrote. One can access this applet in several ways. One address is

<http://mcbilliards/sourceforge.net/Deg100/>

Another address is my website:

<http://www.math.brown.edu/~res/Java/App46/test1.html>

This applet is a toy version of McBilliards specifically designed for the 100 Degree Theorem. The Java applet displays the polygons P_3, \dots, P_{221} . One can zoom into the picture to see the fine structure of these polygons.

1. For each $j = 7, \dots, 221$. a click on the polygon P_j calls forth display of the vertices of the polygon, and also the word W_j and its unfolding. One can drag the mouse around P_j and check visually that (modulo roundoff error) $P_j \subset O(W_j)$.
2. We break P_5 into two regions P_{51} and P_{52} . One can click on each of these regions and see the vertices and corresponding words W_{51} and W_{52} as above. (These regions are not actually named in the program.)
3. We do the same for P_4 as we do for P_5 , using sub-regions P_{41}, \dots, P_{45} .
4. For $j = 3$ and $j = 6$, we break P_j into an infinite number of smaller polygonal regions. In each case, one can see the words corresponding to the first 10 regions. We show enough so that the pattern is fairly clear. Again, for these first few words, one can verify visually that the polygonal region is contained in the corresponding orbit tile.

The words and polygon vertices are displayed in full, so that (modulo the reader being able to fill in several infinite patterns from a finite start) the complete record of the words and polygons resides in the applet.

7.2 The Basics of the Main Program

Probably the most durable location for McBilliards is the website

<http://mcbilliards.sourceforge.net>

One can download McBilliards from this website. One can also run McBilliards as an applet from the website, though this doesn't work with all browsers. Another place to run McBilliards on the web is

<http://www.math.brown.edu/~res/Java/App47/A2.html>

Accessing the Documentation: The first thing to do is to see how the documentation for the program works. For example, there is a little black box with a question mark at the very bottom right of the program. If you click on this box (or any other box that has a question mark in it) the documentation window will pop up. Most of the features of McBilliards have a question box beside them, so that you can learn what they do and how to use them.

The Mouse Emulator: The mouse emulator lives at the bottom right of the program. The question box we mentioned above pertains to this module, and explains how to use the mouse emulator. McBilliards is meant to run with a 3 button mouse. If you don't have a 3 button mouse, or if your browser does not interpret your mouse clicks correctly, you can get around the problem by using the mouse emulator on the bottom right. By clicking on the question box, you can see how to operate the emulator.

Parameter Selection: The big central window in McBilliards is the parameter window. This window contains the region Δ we have discussed in the paper. You select points on this window by clicking button 2 of the mouse over a point. You can also drag the mouse – again button 2 – to select a point. If you want to see the triangle that your selection corresponds to, click on the “more popups” window at the top of the program. This brings up an auxilliary menu. From this menu, click on the “billiard path” option. This brings up another window that displays the triangle corresponding to the point in parameter space you have selected. This auxilliary window also displays billiard paths in the triangle, hence the name.

Searching: Once you have selected a point you like, you can press the “seek” button at the bottom of the program. This will find all the stable words less than the displayed length. We initially set the program to 50. We recommend that you choose a point on the obtuse side that is fairly near the right-angled line. If you pick a point too far into the obtuse region, your search won’t turn up anything (unless you increase the maximum word length.) When your search is done, an auxilliary window pops up, displaying all the hexpaths of the words you have found.

Plotting: Once you have selected a point and done a search, you can select one of the hexpaths from the auxilliary window that has popped up. After you select one of these hexpaths, you can plot the corresponding orbit tile by pushing the plot button. The color selector allows you to change the color of the plotted tile. The bottom left portion of the program gives you some buttons for managing the plotted tiles – deleting, raising, and recoloring.

Unfolding Window: Once you have plotted an orbit tile (or before) you can click on the top of the program to bring up the unfolding window. The unfolding window draws the unfolding $U(W, T)$, where W is the currently selected word and T is the currently selected triangle. By dragging the mouse around an orbit tile, you can see the unfolding change with the point selection. This is a powerful sanity check that the searching and plotting options are working correctly. Like almost all the windows on McBilliards, the unfolding window is resizeable. You can see a nice large picture of the unfolding if you like.

Word Window: Clicking at the top of the program brings up the word window. This shows a large copy of the hexpath for the current word. The word window is animated, so one can see how the hexpath is created from the word.

The best way to get a feel for the basic features of McBilliards is to play with the program – i.e. search, plot, survey tiles – with both the word and unfolding windows open. The unfolding and word windows have many auxilliary features embedded in them, and in time the use can learn these from the documentation. We will talk more about the unfolding window below.

7.3 The Unfolding Window: More Details

Now we will assume that you have mastered the basic features of McBilliards, discussed above. Here we discuss the unfolding window in more detail.

Turning Pairs: If you click the middle mouse button on an edge of the unfolding, you can see the turning pair of that edge displayed at the left. The turning pairs were discussed in §2.4. This will give you a better feel for the algorithm presented in §2.4.

Defining Functions: You can select a pair of vertices from the unfolding that is drawn in the unfolding window. Once you select these vertices, the unfolding window computes the defining function associated to these vertices. The defining function is then displayed at the bottom of the unfolding window, using the conventions described in §2.7. One funny feature is that positive numbers are displayed in which and negative numbers are displayed (without signs) in black. We somewhat regret this convention now, but it does save space. As an aid to the computation of the defining function, the unfolding window also shows the path of edges connecting the one vertex to the other, as discussed in Lemma 2.7.

The Leading Vertices: One can also access the defining functions in another way. One can turn on the “compute leaders” option on the unfolding window. Assuming that you have plotted a tile, the unfolding window will automatically select and display the pair of vertices on the unfolding, one top and one bottom, that come closest to having the same height. In this way, you can see which defining functions define the edges of the tile.

Derivative Bounds: Once a defining function is computed, the derivative bounds discussed in §4.1 are displayed at the bottom of the unfolding window. The documentation for this part of the unfold window has more information.

7.4 Surveying our Proof

One can survey our proof using a version of our applet that we have “embedded” into McBilliards. One accesses this embedded version of the applet by bringing up the “more popups” menu and selecting the “100 degree result”

window. This brings up the embedded copy of the applet. Using the “100 degree result” window, you can survey our computational algorithm down to the last detail. (This is extremely tedious, but possible.) Here we explain how one surveys the results of the tournament algorithm, discussed in §4.

- To run the verify algorithm for a particular word, select the *verify single* mode on the 100 degree window interface and then click on the desired word. (These words are indexed by little square buttons on the interface.) Be sure to have the *trace verify* button off.
- Once the picture is plotted on the main McBilliards window, turn on the *trace verify button* and select your favorite dyadic square that you have just plotted by clicking inside it. Now click on the same word you just clicked.
- With the *trace verify* mode on, McBilliards re-runs the algorithm, discarding any square which does not contain the selected point. This has the effect of just tracing through the part of the algorithm which deals with the selected square.
- Open up the unfolding window after the selected square has been plotted. Along the bottom of the square you will see three kinds of boxes: the top winners, the bottom winners, and the tournament record. The tournament record consists of a bunch of pairs of the form (p, q) , where p loses to q on some box which contains the selected one. We call these *match boxes*.
- If you click on one of these matchboxes, you will see the formulas for the defining function associated to the relevant pair of vertices. You also get to see a graphical display of the gradient and the quadrant which contains the gradient throughout the dyadic square. By moving the point around on the main interface, you can visually check that the gradient remains within the quadrant. Also, you see displayed all the quantities which go into the calculation of the certificates, so you can recompute them yourself from the information.
- If you click on every single match box and make the computations yourself, by hand, you will have given your own proof that the tournament has performed correctly. Finally, you can go through all the pairs of the form (top winner, bottom winner) and make all the same checks.

7.5 Surveying McBilliards as a Whole

This section is for the diehard computer enthusiast. Going back to the sourceforge McBilliards webpage, you can browse through our online documentation for McBilliards, which shows the details of essentially class, method, and interface in McBilliards.

The code relevant to the 100 Degree Theorem only takes up a small subset of the total program. To isolate the relevant code, we have put it in files which have the Deg100 prefix, such as Deg100Verifier.java. However, there are some basic classes, such as the complex number class and some graphics classes, which are required to support the code in the Deg100 files.

8 References

- [**BGKT**] M. Boshernitzyn, G. Galperin, T. Kruger, S. Troubetzkoy, *Periodic Billiard Trajectories are Dense in Rational Polygons*, Trans. A.M.S. **350** (1998) 3523-3535
- [**G**] E. Gutkin, *Billiards in Polygons: Survey of Recent Results*, J. Stat. Phys. **83** (1996) 7-26
- [**GSV**], G.A Galperin, A. M. Stepin, Y. B. Vorobets, *Periodic Billiard Trajectories in Polygons*, Russian Math Surveys **47** (1991) pp. 5-80
- [**H**] W.P. Hooper, *Periodic Billiard Paths in Right Triangles are Unstable*, Geometriae Dedicata (2006) to appear
- [**HH**] L.Halbeisen and N. Hungerbuhler, *On Periodic Billiard Trajectories in Obtuse Triangles*, SIAM Review **42.4** (2000) pp 657-670
- [**HS**] W.P. Hooper and R.E. Schwartz, *Billiards in Nearly Isosceles Triangles*, preprint 2008
- [**M**] H. Masur, *Closed Trajectories for Quadratic Differentials with an Application to Billiards*, Duke Math J. **53** (1986) 307-314
- [**MT**] H. Masur and S. Tabachnikov, *Rational Billiards and Flat Structures*, Handbook of Dynamical Systems 1A (2002) editors: B. Hassleblatt and A. Katok
- [**S**] R. Schwartz, *Obtuse Triangular Billiards I: Near the (2, 3, 6) Triangle*, Journal of Experimental Mathematics (2006) to appear
- [**T**] S. Tabachnikov, *Billiards*, SMF Panoramas et Syntheses, **1** (1995)
- [**Tr**] S. Troubetzkoy, *Billiards in Right Triangles*, preprint 2004.
- [**V**] W. Veech, *Teichmuller Curves in Moduli Space: Eisenstein Series and an Application to Triangular Billiards*, Invent Math **97** (1992) 341-379

[W] S. Wolfram, *Mathematica: A System for Doing Mathematics by Computer*, Wolfram Press (2000)